Universidad Autónoma de Madrid
Escuela politécnica superior

Grado en Ingeniería de Tecnologías y Servicios de Telecomunicación

TRABAJO FIN DE GRADO

DESARROLLO DE UNA ANTENA DE BOCINA CORRUGADA PARA UN RADAR MONOPULSO EN LA BANDA L

Author: Andreea Simona Palade
Supervisor: Korbinian Schraml
Co-Supervisor: José Luis Masa Campos

DEVELOPMENT OF A CORRUGATED HORN ANTENNA FOR MONOPULSE RADAR AT L-BAND

Author: Andreea Simona Palade
Supervisor: Korbinian Schraml
Co-Supervisor: José Luis Masa Campos

IHF - Institute of High Frequency Technology
RWTH Aachen University
Germany
December 2017

Abstract

The mono-pulse tracking and imaging radar (TIRA) is a space observation radar which uses a four-pyramidal-horns array to feed the reflector of the system. The radiation pattern of the array has too high side lobes, causing a high radiation power below the safety limits. The aim of this thesis is to study if with four-corrugated-horns array, lower side lobes can be achieved.

First of all, the design of a corrugated horn antenna is carried out. The antenna operates in L-band, at 1.3 GHz. As the ultimate purpose of the horn is being used in a monopulse radar, the basis of this type of radar are firstly described. In order to correctly estimate the dimensions of the antenna, the theoretical background of corrugated horns is described.

Following, the development of the antenna is detailed. In the first place, the sizes of the horn are estimated, supposing that it is optimum. Secondly, the dimensions of the corrugations are calculated, including their depth. It is important to define a coordinate system for the corrugations in order to generate the horn in CST, and compute their coordinates and the coordinates of the waveguide.

Regarding the depths of the corrugations, the combination of depths that maximize the performance of the system is attempted to find. To this aim, a parameter sweep is performed for the depth of each corrugation. The results of this process are compared with the results of a genetic algorithm optimization. Then, the influence that the number of corrugations have on the performance of the system is analized. For this purpose, two new horn models are developed: one with the minimum number of corrugations possible and another one with more corrugations than the first one. These three systems are analized and compared.

Finally, three antennas arrays are generated: one for each type of horn. The performance of each system is analized and the radiation patterns are compared with the radiation patterns of the TIRA reference.

Resumen

El radar monopulso TIRA (Tracking and Imaging Radar) es un radar de observación espacial en el que se usa un array formado por cuatro antenas de bocina piramidal para alimentar el reflector del sistema. Este radar tiene una limitación: su potencia de radiación está por encima de los límites de seguridad débido a que el nivel de los lóbulos secundarios del diagrama de radiación del array es muy alto. Este Trabajo Fin de Grado estudia si es posible reducir el nivel de los lóbulos secundarios del diagrama de radiación del array, empleando una antena de bocina cónica corrugada para el array.

En primer lugar, se describen las principales características de un radar monopulso y de una antena de bocina cónica corrugada. Después, se lleva a cabo el diseño de la bocina, teniendo en cuenta que ésta opera en la banda L, a 1.3 GHz.

A continuación, se explica detalladamente el desarrollo de la antena. En primer lugar, se calculan las dimensiones de la antena de bocina suponiendo que es óptima. En segundo lugar, se define un sistema de coordenadas para las corrugaciones y se calculan sus dimensiones.

En cuanto a la profundidad de las corrugaciones, se busca la commbinación de profunidades que maximiza el rendimiento del sistema. Esto se hace de dos formas: manual, mediante un barrido para cada parámetro, y de forma automática mediante una optimización empleando el algoritmo genético. Después, se estudia que influencia tiene el número de corrugaciones sobre el rendimiento del sistema. Para ello, se desarrollan otras dos bocinas: una con el mínimo número de corrugaciones posible, y otra, con más corrugaciones que la primera.

Finalmente, se generan tres arrays de antenas: uno para cada tipo de bocina. El diagrama de radiación de cada array se analiza y se compara con el diagrama de radiación del array empleado en el radar TIRA.

Key words

Monopulse Radar, TIRA, Antenna, Horn, Conical Horn, Corrugated Horn, Corrugations, Genetic Algorithm, Optimization, Array, Radiation Pattern.

Palabras clave

Radar Monopulso, Antena, Antena de bocina, Bocina cónica, Bocina corrugada, Corrugaciones, Algoritmo Genético, Optimización, Array, Diagrama de Radiación.

Acknowledgement

I would first like to thank to my thesis supervisior Korbinian Schraml, for giving me the chance to do this Bachelor thesis, for all the new things I have learned and for all his support and advices.

Thanks to Cosme Culotta-López to make it possible to come to Aachen, for giving me all the information I needed in order to organize and carry out this exchange program.

Thanks to José Luis Masa Campos for being my co-supervisor and for helping me with the administrative process.

Furthermore I would like to thank to Professor Heberling for giving me the opportunity to do this project in the Institut für Hochfrequentztechnik in RWTH Aachen University.

Finally, I would like to thank to my loved ones, to my family and friends who have supported me throughout all these years, for encouraging me, for being by my side, for never giving up on me and for never letting me to give up.

Contents

List of Figures

List of Tables

1 Introduction

1.1 Motivation

The mono-pulse tracking and imaging Radar (TIRA) is a space observation radar located at the Fraunhofer Institute for High Frequency Physics and Radar Techniques in Germany. The system serves as the central experimental facility for the development and investigation of radar techniques for the detection and reconnaissance of objects in space. TIRA can measure the orbit with high precision or produce a high resolution image of objects such as satellites.

The radar operates in L-band for tracking and debris detection at 1.3 GHz. For imaging it operates in Ku-band at 16.7 GHz. The system uses a 34 metres diameter horn antenna to feed a reflector (Figure 1.1). The antenna can be turned 360°in azimuth and 90°in elevation [1].

The antenna system used to feed the reflector is a 2x2 array formed by four smooth-wall pyramidal horns. This array has a drawback: the side lobe level of its radiation pattern is too high. The radiation power is too high and it is below the safety limits. This thesis studies if with an array formed by four corrugated horns lower side lobes can be achieved and therefore if there is possible to transmit more power within the safety limits.

Figure 1.1: Insight into space observation radar TIRA

Source: [1]

1.2 Goals

The main goal of this thesis is the design of a corrugated horn antenna. For this purpose, the dimensions of the horn antenna are calculated in the first place. Then, a coordinate system is defined in order to correctly place the corrugations in the plane and their dimensions, as their length and the distance between them, are computed.

The next goal is to estimate the depths of the corrugations that maximize the gain of the system. To achieve this, several parameter sweeps and two genetic algoritm optimizations have been done.

Following, it is analized what number of corrugations should have the horn to achieve a better system performance.

Finally, three antenna arrays are generated and the last goal is to compare the radiation patterns of this arrays with the radiation patterns of the TIRA Reference.

1.3 Outline

This document has the following outline:

- **Chapter 1: Introduction** - In this chapter, the motivation, the goals and the outlines of the thesis are described.
- **Chapter 2: State of the art** - First, the fundaments of the monopulse radar are introduced in this chapter. Secondly, the types of aperture antennas are listed and next, horn antennas basis are explained. Then, conical and corrugated horn antennas are gone into in more detail, since all the concepts presented are used throughout the document.
- **Chapter 3: Antenna design** - In this chapter all the procedures that have been followed in order to generate the antenna are described step by step. First of all, the conical horn design, then the corrugations design, including their coordinate system and their depths. After that, the impact which the number of corrugations have on the horn is analized, and two new horn models are proposed. Next, an array is generated and finally a comparison between the radiation patterns of the array and the TIRA reference is made.
- **Chapter 4: Conclusions** - This chapther draws the conclusions based on these analysis and arises the future work.

2

State of the art

2.1 Monopulse radar

A radar system is often used for tracking. It determinates the current and future position of a target by measuring its coordinates [2]. With the monopulse radar, the angular position of a target can be obtained from only one pulse, as its name indicates. In order to find out the direction to target, two important techniques have been developed: the **amplitude-comparison method** and the **phase-comparison method**.

The amplitude-comparison monopulse uses two intersecting antenna radiation patterns separated by an angle $\pm\theta_s$ from the equisignal direction. Both sum and difference patterns are used on reception, while only the sum pattern is used on transmission . The sum signal is used for range measurment. If the amplitudes of the antennas patterns are rested, the result will be the magnitude of the target deviation from the equisignal direction, and its sign indicates the direction of the displacement. The difference will be zero when the equisignal direction and the target coincide [2], [3].

As explained in [3], additions and subtractions between signals and scalar multiplications are made by converters after the signals have been amplified. The converters and amplifiers are contained in the angular discriminator. There are three types of angular discriminators: **amplitude discriminator**, responding only to amplitude ratios, **phase discriminator** reacting only to phase ratios and **sum-difference discriminator**, used for both amplitude and phase ratios and also for adding and substracting operations. In Figure 2.1 are shown the raddiation patterns of an amplitude-comparison monopulse system with sum-and-difference angle discriminator. The reference system axis for the measurment is θ_0. The main beams directions of the two antennas are separated by the angle θ_s. These patterns are added and subtracted. The result of the subtraction is $\Delta\theta$, the magnitude of the angle error [4].

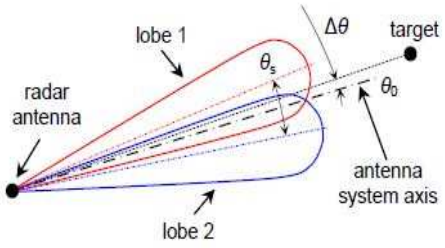

Figure 2.1: Partial antenna patterns for amplitude sum-and-difference monopulse system.

Source: [4]

The phase-comparison monopulse compares the phases of the signals received by two antennas in order to determine the direction to target. The farfield radiations have equal magnitude in space, hence the reflected signals have the same amplitude, but different phase. Figure 2.2 shows two antennas separated by a distance d. θ is the angle between the line of sight of the target and the x-axis. The line joining the two antennas is perpendicular to the x-axis. The distance from *Antenna 1* to the target is $R_1 = R + \frac{d}{2}\sin\theta$ and the distance from *Antenna 2* to the target is $R_2 = R - \frac{d}{2}\sin\theta$. The phase difference between the signals is $\Delta\varphi = \frac{2\pi}{\lambda} d \sin\theta$ [2].

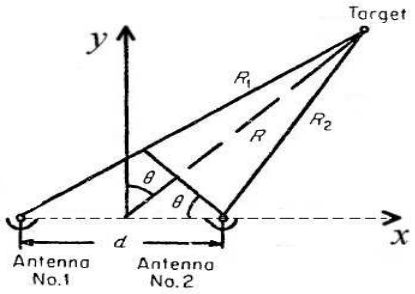

Figure 2.2: Determinating angular coordinates for phase-comparison monopulse system.

Source: [3]

A monopulse system consists of three basic elements which appear in Figure 2.3. The angle-data transmitter provides information about the angular position of the target. It is the antenna of the monopulse system. The information converter converts the signal parameter ratios, and the angular discriminator provides the angle measurment [3].

Figure 2.3: Block diagram of a monopulse system

Source: [3]

2.1.1 Phased Antenna Arrays

A phased antenna array is a set of antennas which generates a radiation pattern whose shape and direction depends on every single element of the array. The main advantage of using antennas arrays in radar systems is that they offer the possibility to control the direction of the radiation by varying the relative phases of each individual antenna. This can be done through electronic control.
The distance between elements should be $\frac{\lambda}{2}$ in order to obtain the smallest side lobes. If the distance is greater than $\frac{\lambda}{2}$, grating lobes may appear.
If the radiation pattern of an array has only one beam, phase switchers can be added at the end of each antenna. One additional beam will appear for every phase switcher inserted and the result will be a multi-beam antenna. For an amplitude-comparison monopulse system, after being amplified the signals are fed to two phase switchers, forming two beams. The signals from the outputs of the phase switchers are fed to the summator. For a phase-comparison monopulse system, two radiation patterns are formed by adding the signals from each half of the array. [3].

2.1.2 Antenna Feeds on Monopulse Radar

For an antenna array feeding a reflector formed by four horns, the direction to target can be determinated by comparing paired sums of signals. For instance, with the irradiator arrangement shown in Figure 2.4, the greatest propagation is obtained. If the sum of signals (1+2) is compared with (3+4), elevation will be measured, and if (1+3) is compared with (2+4), azimuth will be measured.

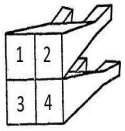

Figure 2.4: A four-horn irradiator

Source: [3]

The horns are excited according to the diagram showed in Figure 2.5. The waveguide bridges are used at the points indicated in the diagram. On the first two bridges, the signals (1,3) and (2,4) are summed in pairs and then added in bridge III forming the sum signal $\sum$. In bridge III the sum of the signals (2,4) is subtracted from the sum of the signals (1,3), forming the difference signal Δ with respect to azimuth. The difference signal with respect to elevation is obtained by adding in the bridge IV the difference of signals (1,3) and (2,4), obtained on the first two bridges. This gives the required result because the system is linear and the associative law is applicable to it $(1-3)+(2-4)=(1+2)-(3+4)$. In order to form the sum radiation pattern, the shaping circuit of the irradiating system excites in phase all four-horns. In order to obtain the most optimal radiation, horn dimensions are selected so that in the formation of the sum beam the antenna has maximum amplification with uniform irradiation of the mirror [3].

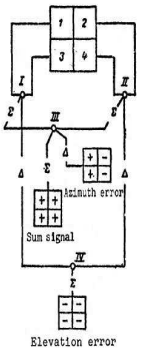

Figure 2.5: Excitation diagram of a four-horn irradiator

Source: [3]

2.2 Aperture antennas

An aperture antenna is an antenna with an aperture at the end through which radiates energy in one specific direction. It is most commonly used at microwave frequencies.
The aperture can be square, rectangular, circular, elliptical, or it can take any other shape. Some apertures are delimited by conductive metal walls, as the slot antenna in Figure 2.6a or the horn antenna in Figure 2.6b. Other ones, such as reflector antennas in Figure 2.6c and lens antennas in Figure 2.6d, are defined as a portion of a flat front surface in which the fields of the wave collimated by it takes significant values.
Aperture antennas are most commonly used for aerospace applications because they can be inserted into the spacecraft or aircraft surface [5], [6].
This thesis is focused on a horn antenna.

(a) Slot Antenna

(b) Horn Antenna

(c) Reflector Antenna

(d) Lens Antenna

Figure 2.6: Aperture Antennas

Source: [6]

2.3 Horn antennas

2.3.1 Introduction

The horn antenna can be defined as a section of waveguide where the open end is flared in order to adapt the radiant medium to the feeding waveguide [6]. The flared portion can be square, rectangular, or conical and its type, direction, and amount can have a deep effect on the general performance of the element as a radiator.
The maximum radiation corresponds with the axis of the horn. The horn is usually fed with a waveguide, which can be rectangular or circular. In Figure 2.7 different types of horn antenna are shown.

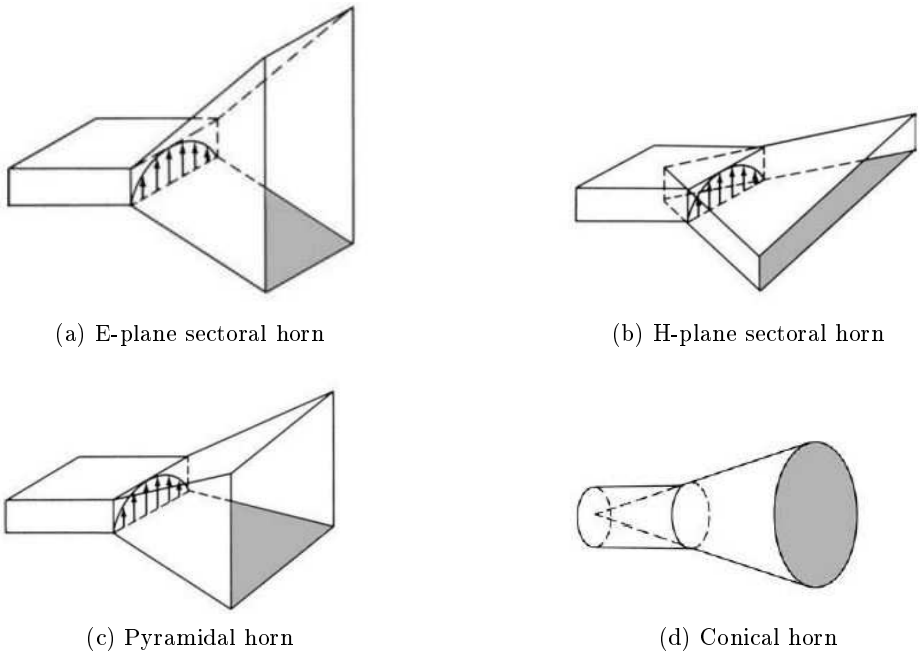

(a) E-plane sectoral horn

(b) H-plane sectoral horn

(c) Pyramidal horn

(d) Conical horn

Figure 2.7: Horn Antennas

Source: [7]

The horn antennas are very popular for space and ground-based antenna systems because they are easy to manufacture and RF losses are low even at millimeter and submillimeter frequency ranges. They can reach high gains and high bandwidths, they are easy to excite and very versatile.
The horn is most commonly used to feed reflectors and lenses. It is a common element of phased arrays and serves as a universal standard for calibration and gain measurements of other high gain antennas.
The horn is used in large radio astronomy, satellite tracking, and communication dishes installed throughout the world [5].

2.3.2 Conical horn

Conical horns are usually feed with circular waveguides. A big advantage of the circular waveguide is that it allows any type of polarization. The geometry of the conical horn is shown in Figure 2.8, where a is the radius of the circular waveguide aperture, R_c is the slant radius, more specifically the distance between the waveguide-horn junction and the sides of the horn, L_c is the axial length, in other words the distance between the center of the aperture and the junction, A is the radius of the aperture and γ_c is the semiflare angle [8].

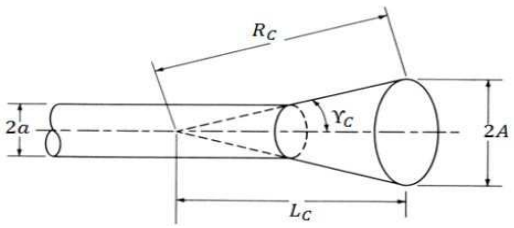

Figure 2.8: Conical horn geometry

Source: [7]

The maximum quadratic phase error is $s = \frac{A^2}{2\lambda_0 L_c}$. The normalized radiation pattern for the E-plane is illustrated in Figure 2.9 and for the H-plane in Figure 2.10, both without the obliquity factor $\frac{1+\cos\theta}{2}$ [6].

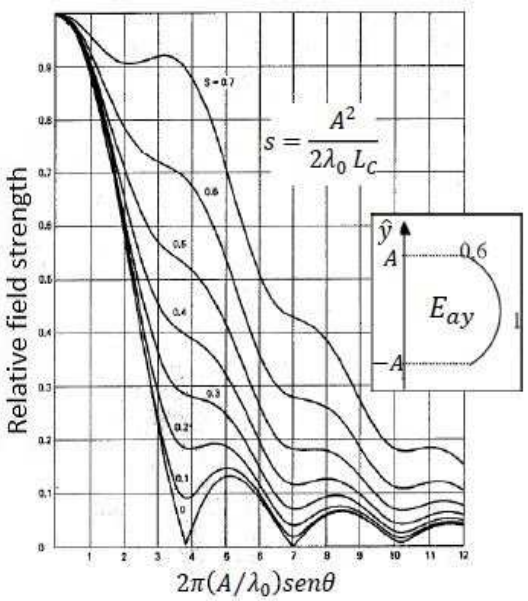

Figure 2.9: E-plane

Source: [7]

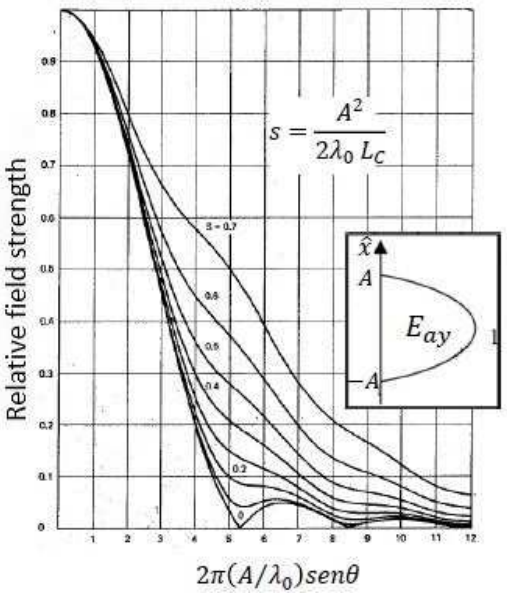

Figure 2.10: H-plane

Source: [7]

In Figure 2.11 is shown the directivity of a conical horn as a function of the aperture diameter and for different axial horn lengths. As it can be observed, as the flare angle increases, the directivity of the horn increases and after it hits a maximum point, it starts to decrease due to the dominance of the quadratic phase error at the aperture [7].

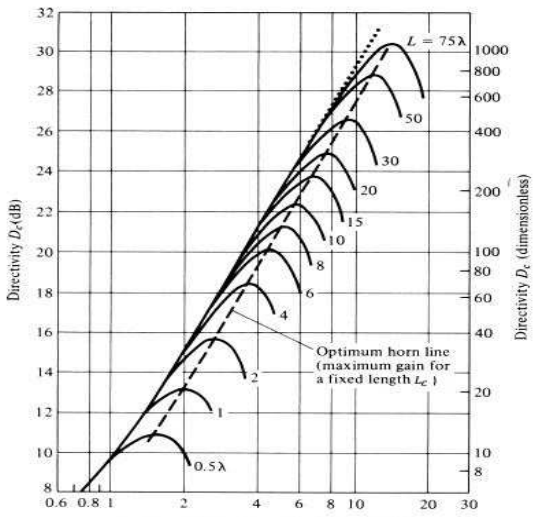

Figure 2.11: Diameter of horn aperture 2A(wavelengths)

Source: [7]

The directivity of a conical horn is optimum when its radius is equal to $A = \frac{\sqrt{3\lambda_0 L_c}}{2}$, which corresponds to a maximum quadratic phase error $s = \frac{3}{8}$ and an aperture efficiency around 51% [7]. If the aperture of the horn is flat and uniform illuminated, the aperture efficiency will be of

100% [6]. Consequently, the gain will be equal to the directivity: $G_0 = D_0 = \frac{4\pi}{\lambda_0^2} A_{aper}$, where A_{aper} is the area of the aperture. For a circular aperture, $A_{aper} = \pi A^2$, where A is the radius of the aperture. Hence, the gain will be: $G_0 = \frac{4\pi^2 A^2}{\lambda_0^2}$. Therefore, the directivity of the horn increases when the radius of the aperture increments.

2.3.3 Corrugated horn

When the smooth-wall horn is used as a feeding element for a reflector, it leads to astigmatism, which consists in unequal phase centers in orthogonal planes. For dual linear or circular polarization, the horn aperture must be square or circular and the beamwidths in the E-plane and H-plane are not equal. Furthermore, the sidelobes in the E-plane are higher than in the H-plane. Finally, the diffraction of the E-plane walls causes backlobes. All these problems can be eliminated by corrugating the walls [8].
Concerning the efficiency, with smooth-wall horns aperture efficiencies of 50-60% can be obtained, while with corrugated horns efficiences of the order of 75-80% can be achieved. Compared with a smooth-wall horn, a corrugated horn has larger 3 -dB beamwidth, a lower 10 -dB beamwidth and lower levels of the minor lobes and back lobes. The corrugations placed on the walls perpendicular to the E field of a horn transform the electric field distribution in the E-plane from uniform at the waveguide-horn junction to cosine at the aperture.
Figure 2.13 shows a corrugated pyramidal horn, with corrugations in the E-plane walls. In the H-plane, normaly there are not corrugations, as diffractions at the edges of the aperture in this plane are insignificant. As showed in Figure, there are two types of corrugations: perpendicular to surface and perpendicular to axis[7]. In Figure 2.14 a conical corrugated horn, also denominated scalar horn can be seen.
In this thesis a conical corrugated horn with corrugations perpendicular to axis is developed.

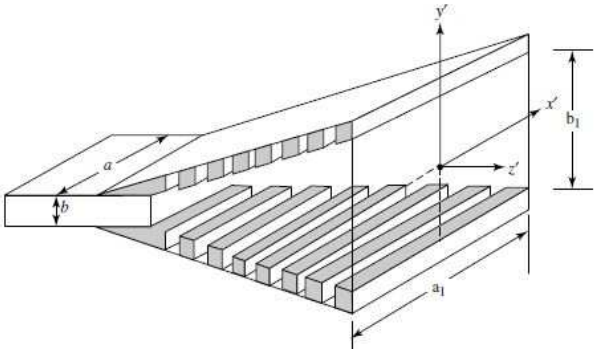

(a) Corrugated pyramidal horn

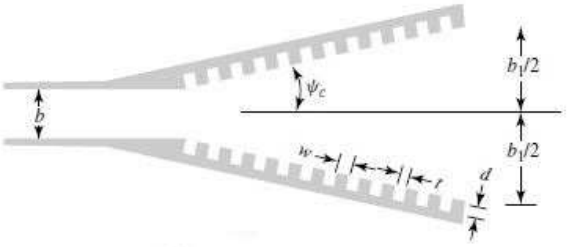

(b) E-plane

Figure 2.12: Corrugated pyramidal horn with corrugations in the E-plane

Source: [7]

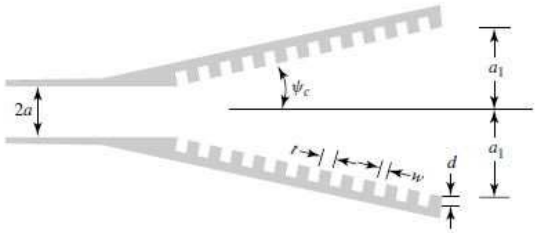

(a) Corrugations perpendicular to surface

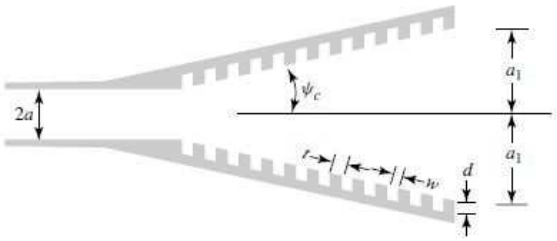

(b) Corrugations perpendicular to axis

Figure 2.13: Types of corrugations

Source: [7]

Figure 2.14: Scalar horn

For an efficient design, it is necessary to use 10 or more corrugations per wavelength[7]. According to [7], to simplify the analysis of an infinite corrugated surface, it will be assumed that:

1. **The teeth of the corrugations are very thin.**
2. **Reflections from the base of the corrugation are only those of a TEM mode.**

Moreover, the second assumption is valid only if the width of the corrugations w is small enough compared to the free-space wavelength λ_0 and the depth of the corrugations d. The assumption will be: $w < \frac{\lambda_0}{10}$.

If a corrugated surface complies with the specified assumptions, its aproximate surface reactance will be:

$X = \frac{w}{w+t}\sqrt{\frac{\mu_0}{\epsilon_0}}\tan(k_0 d)$, when $\frac{w}{w+t} \cong 1$, which can only be satisfied if $t < \frac{w}{10}$.

It is important that the surface reactance of corrugated surfaces is capacitive, to annul the tangential magnetic field parallel to the edge at the wall. Consequently, these surfaces will not support surface waves, will prevent illumination of the E-plane edges, and will reduce diffractions. This can be accomplished if $\frac{\lambda_0}{4} < d < \frac{\lambda_0}{2}$. If $d < \frac{\lambda_0}{4}$ or $d > \frac{\lambda_0}{2}$, the surface reactance will be inductive, and if $\frac{3\lambda_0}{2} < d < \lambda_0$ will be capacitive again, but this interval is not so commonly used. Furthermore, the corrugations need to be $\frac{\lambda_0}{4}$ at the aperture since a $\frac{\lambda_0}{4}$ corrugation depth balances TM_{11} and TE_{11} modes coexisting and gives better results. Before

the aperture the corrugations depth must be higher than a quarter-wavelength, otherwise there will be mismatching in the transition region, where the TM_{11} mode is generated from the TE_{11} mode. On the other hand, if depths are approximately $\frac{\lambda_0}{2}$, their influence on the matching will be negligible [8]. Moreover, the cutoff depth depends on the corrugation width w, but its effect is insignificant if $w < \frac{\lambda_0}{10}$ and $\frac{\lambda_0}{4} < d < \frac{\lambda_0}{2}$ [7].

In addition, if the corrugations are very close to the waveguide-horn junction, they will affect the impedance and VSWR of the antenna. In order to avoid this, the first corrugation must be placed at a small distance away from the junction [7].

3

Antenna Design

3.1 Introduction

In this chapter, the antenna design is described step by step. The design specifications are shown in Table 3.1. The L-band goes from 1 to 2 GHz and the central frequency of the system is 1.3 GHz.
First, the dimensions of the horn as the axial length, the radius of the aperture, the slant radius, the semiflare angle and the dimensions of the waveguide are calculated. Secondly, the dimensions of the corrugations are estimated and then their coordinate system, more specifically, the coordinates of each point of each corrugation. Continuing, a series of simulations are performed in order to find the depths which maximize the gain of the system. Next, the effect that the number of corrugations have on the system is studied. To this aim, two more horns are created: one with the minimum number of corrugations possible(10), and another one with two more corrugations than the first one. Finally, three arrays are generated, one for each type of corrugated horn. In the end, the resulting radiation patterns are compared with the TIRA reference.

Table 3.1: Design Specifications

Central Frequency	1.3 GHz
Gain	15 dBi
Thickness of the Metal	2.3 mm

3.2 Conical Horn Design

The design which has been realized is optimum in order to achieve the maximum directivity. In Figure 2.8 the geometry of a conical horn was shown. Considering what has been explained in the section 2.3.2 and the design specifications showed in Table 3.1, the dimensions of the horn have been calculated such as indicated in Table 3.2.

Table 3.2: Conical horn dimensions

Parameter	**Symbol**	**Formula**	**Result**	**Units**
Axial Length	L_c	$\frac{G_0\lambda_0}{3\pi^2}$	240.30	*mm*
Aperture Radius	A	$\frac{\sqrt{3\lambda_0 L_c}}{2}$	201.37	*mm*
Slant Radius	R_c	$\sqrt{L_c^2 + A^2}$	313.52	*mm*
Semiflare Angle	γ_c	$atan(\frac{A}{L_c})$	39.96	*degrees*

The circular waveguide is determinated by a length and a radius. In a first approach, a random value proportional to the sizes of the horn was choosen for the length. Respecting the radius of the waveguide, it must be considered that the cutoff frequency for a circular waveguide is $f_c = \frac{1.8412c}{2\pi a}$, where c is the speed of light within the waveguide in *metres per second* and a is the internal radius of the circular waveguide in *metres*. A radius value must be found, so that the central frequency of the system stays between the cutoff frequency of the lowest mode (H_{11}) and the cutoff frequency of the second mode (E_{01}). For instance, if the radius of the waveguide is 80 mm, the cutoff frequency of the lowest mode is 1.09 GHZ and the cutoff frequency of the second mode is 1.3061*1.09 GHz=1.42 GHz.

Table 3.3: Waveguide dimensions

Parameter	**Symbol**	**Value**	**Units**
Waveguide Length	Length_wg	120	*mm*
Waveguide Radius	Rad_wg	80	*mm*

3.3 Corrugations Design

According to section 2.3.3, in Table 3.4 the dimensions of the corrugations have been summarized and calculated in function of λ_0. It is assumed that all the corrugations have the same width(w), and also that they all have the same teeth(t). As the horn must have at least 10 corrugations, as a first approach 12 corrugations have been choosen.

Table 3.4: Corrugations dimensions

Parameter	**Symbol**	**Formula**	**Result**	**Units**
Width of the corrugations	w	$\frac{\lambda_0}{10}$	22.5	mm
Depth of the corrugations at the aperture	d_{aper}	$\frac{\lambda_0}{4}$	56.25	mm
Depth of the corrugations before the aperture	d	$0.4\lambda_0$	90	mm
Teeth of the corrugations	t	$\frac{w}{10}$	2.25	mm
Distance from the waveguide-horn junction	distance	$L_c - (12t + 12w)$	16.52	mm

(a) Lateral view

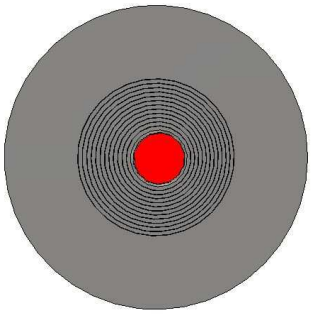

(b) Front view

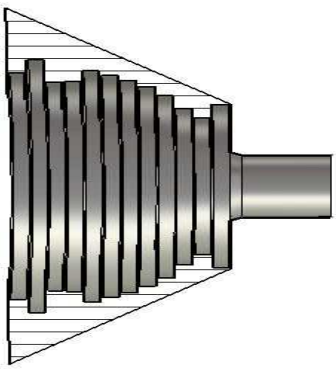

(c) Cross section view

Figure 3.1: View of the horn in CST

3.3.1 Depths Design

In this section several simulations are performed in order to find the combination of depths that maximizes the gain of the antenna. The gain variation with the depth and the 3-dB beamwidth in the E-plane are evaluated for each step.
First, it is assumed that the depth of the first corrugation starting from the aperture is $\frac{\lambda_0}{4}$, as a quarter-wavelength corrugation depth balances the modes coexisting. In the first simulation, in order to observe the behaviour of the system, a parameter sweep is performed for the depths of the rest of the corrugations, supposing that they are equal to each other. In the second simulation, a parameter sweep for the depth at the aperture is performed to demonstrate that the quarter-wavelength corrugation is the best choice. Next, an optimization using the genetic algorithm is runned in order to automatically find the depths that maximize the gain. As the optimization failed, for each corrugation depth a parameter sweep is performed to study if a higher gain can be achieved.

Equal depths before the aperture

For this simulation it is assumed that the depth of the corrugation at the aperture (d_{aper}) is equal to $\frac{\lambda_0}{4}$ and that the rest of the corrugations (from D_2 to D_{12}) have the same depth. A parameter sweep from $\frac{\lambda_0}{4} = 56.25$ mm to $\frac{\lambda_0}{2} = 112.25$ mm is performed in order to find out what depth value provides a better gain and how it affects the 3-dB beamwidth in the E-plane.

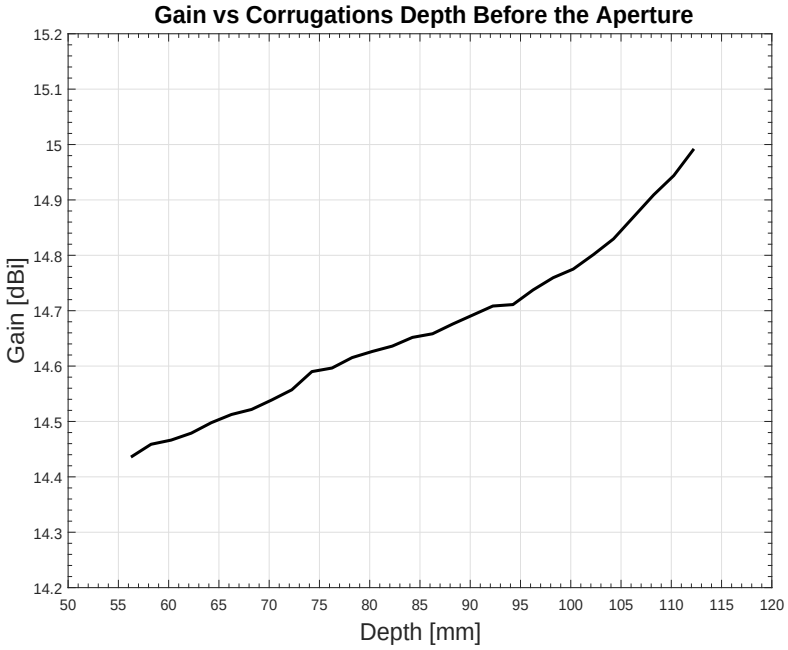

Figure 3.2: Gain vs Corrugations depth before the aperture

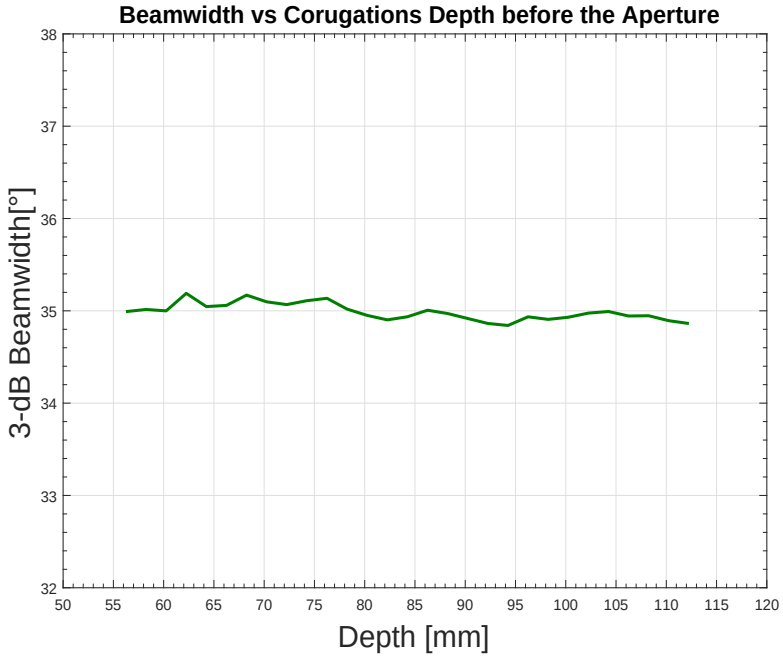

Figure 3.3: 3-dB Beamwidth vs Corrugations depth before the aperture

In Figure 3.2 can be observed that when the depth of the corrugations increases from $\frac{\lambda_0}{4} = 56.25$ mm to $\frac{\lambda_0}{2} = 112.25$ mm, the gain also increases from 14.44 dB to 14.99 dB. For instance, if the depths of the corrugations before the aperture are equal to $0.48\lambda_0 = 108$ mm, the gain will be 14.98 dBi. As it can be seen in the Figure 3.3, as the depth increments, the -3dB beamwidth remains approxiamately constant.

Depth at the aperture

In this simulation it is proved that a quarter-wavelength corrugation depth at the aperture gives the best results. For this purpose, a parameter sweep for the depth of the first corrugation from $\frac{\lambda_0}{4}$ to $\frac{\lambda_0}{2}$ was done in order to study how it affects the gain and the beamwidth. The depths of the rest of the corrugations were not relevant in this case, so all were equaled to a random value closed to $\frac{\lambda_0}{2}$, 108 mm.

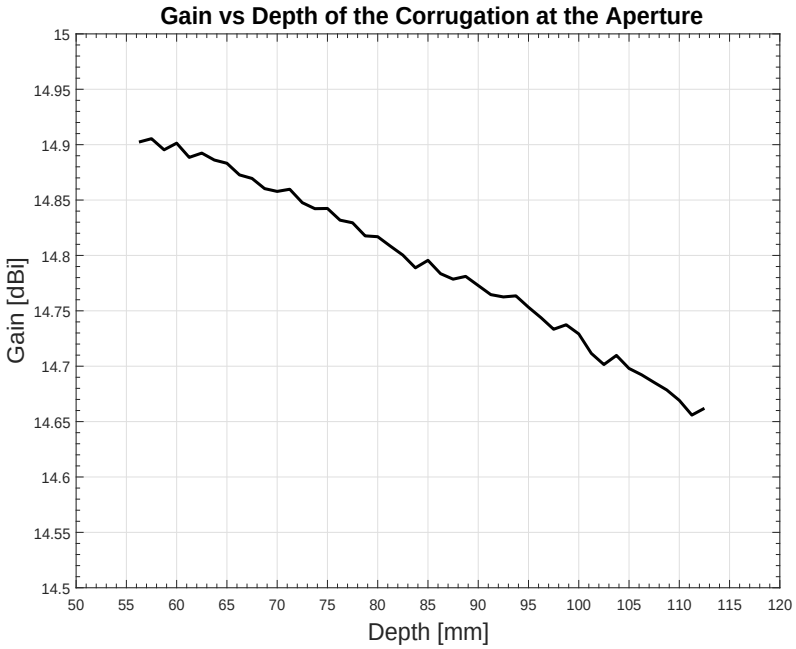

Figure 3.4: Gain vs Depth of the corrugations at the aperture

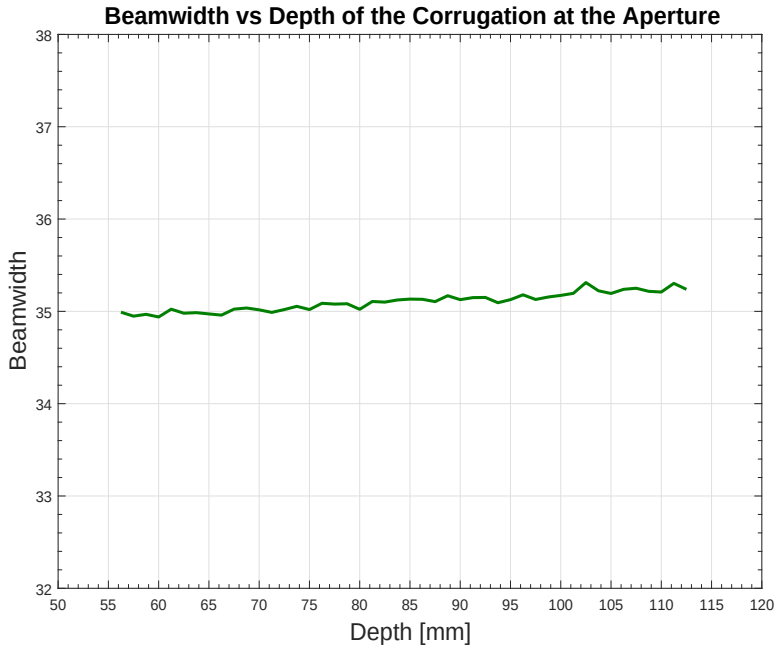

Figure 3.5: 3-dB Beamwidth vs Depth of the corrugations at the aperture

As can be seen in Figure 3.4, the gain decreases from 14.9 dB when the depth is equal to $\frac{\lambda_0}{4}$, to 14.66 dB, when the depth value is $\frac{\lambda_0}{2}$. As shown in the Figure 3.5 there is no significant variation of the beamwidth respect to the depth.

Genetic Algorithm Optimization

An optimization using the genetic algorithm is performed for each depth starting with the second one, in order to find out the corrugations depths that maximize the gain. The first corrugation's depth is fixed to $\frac{\lambda_0}{4} = 56.25$ mm and it will not be changed throughout this paper. The genetic algorithm generates 5 random samples between a specified range($\frac{\lambda_0}{4}$ to $\frac{\lambda_0}{2}$) during 30 generations. The *fitness function* calculates the value of a particular goal (in this case the value of the gain) for each generation and compares the results, keeping the ones which are more close to the goal and in the end, it converges to a global optimum. The results of the optimization can be found in Appendix 3, in the Table 5.

The obtained gain is 14.96 dBi, not higher than the gain obtained before with all the depths equal to each other. Therefore, it can be affirmed that the global maximum was not found. The genetic algorithm may failed because the number of parameters was too large and the range was too high. A parameter sweep is performed next for each corrugation depth to study if a better gain can be reached.

Step-by-step optimization

A parameter sweep from $\frac{\lambda_0}{4} = 56.25$ mm to $\frac{\lambda_0}{2} = 112.5$ mm was done for each corrugation's depth. The gain and the 3-dB beamwidth in the E-Plane are analized in order to observe the performance of the system. In Appendix 2, the results for each corrugation can be found.

In summary, it was observed that the depths of the corrugations have different impact on the gain and on the beamwidth. For example, for the second corrugation, the gain and the beamwidth remain approximately constant while the depth varies, as it can be observed in Figure 3.6.

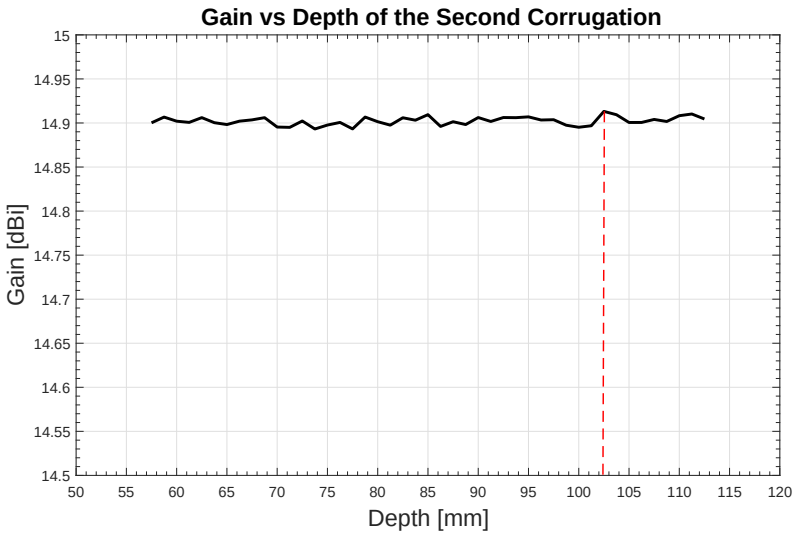

(a) Gain with respect to Depth

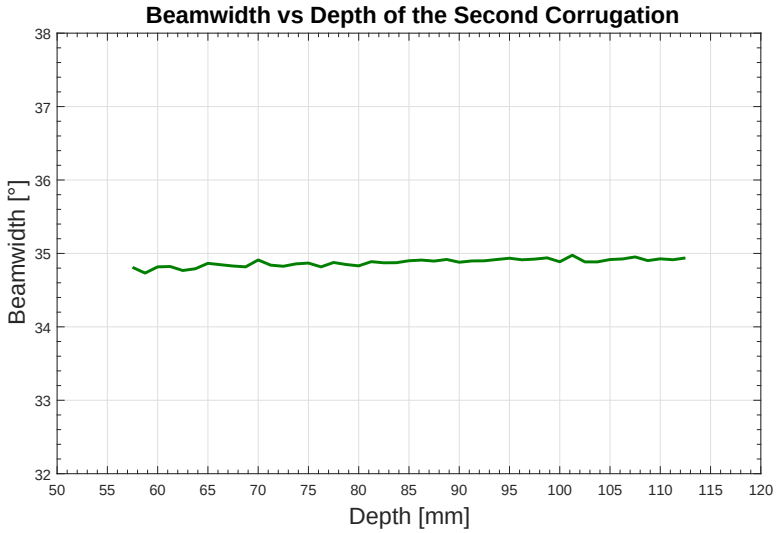

(b) Beamwidth with respect to Depth

Figure 3.6: Gain and Beamwidth of the second corrugation with respect to the Depth

However, for the twelfth corrugation, as it can be observed in Figure 3.7a, the gain increases by 0.9 dBi while the depth increases, and the beamwidth decreases by 3.5°, while the depth increases, as shown in Figure 3.7b.

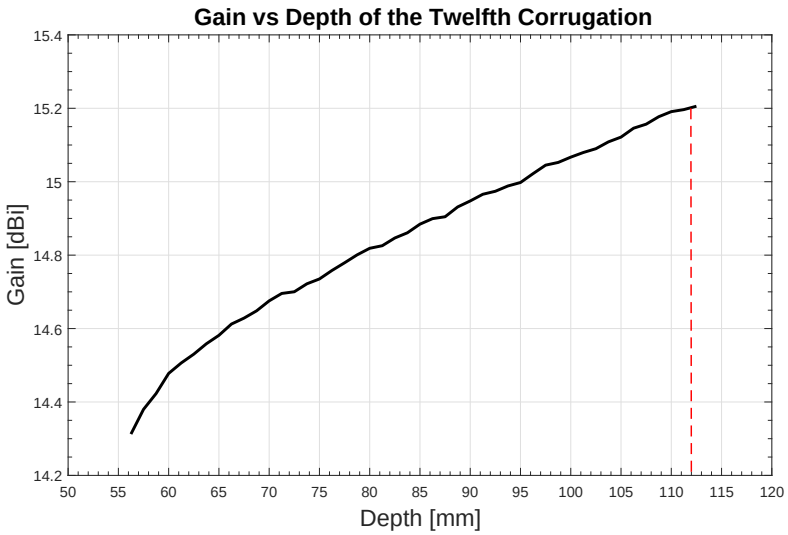

(a) Gain with respect to Depth

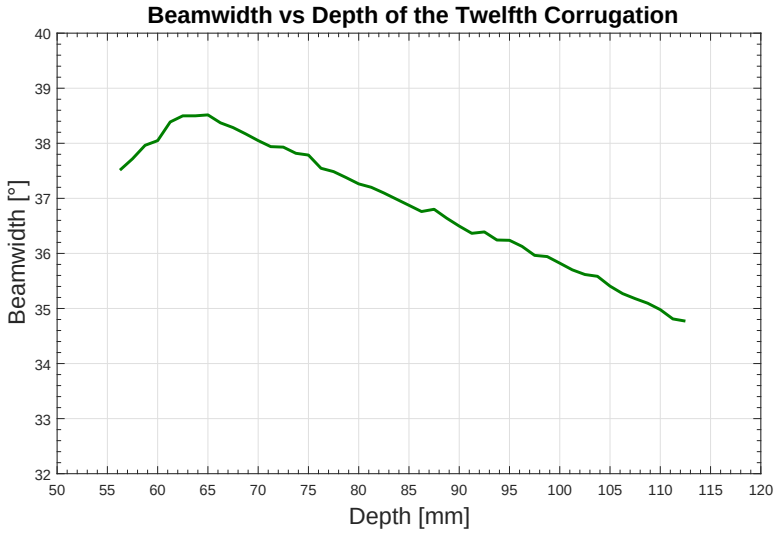

(b) Beamwidth with respect to Depth

Figure 3.7: Gain and Beamwidth of the twelfth corrugation with respect to the Depth

With the step-by-step tunning, the gain obtained is 15.67 dBi, while with the genetic optimization the gain obtained was 14.96 dBi. Next, the system with the maximum depth values found is analyzed. In Figure 3.8 the reflection coefficient is illustrated. It can be observed that the system is matched between 1.21 GHz and 1.72 GHz, obtaining an approximate 510 MHz bandwidth.

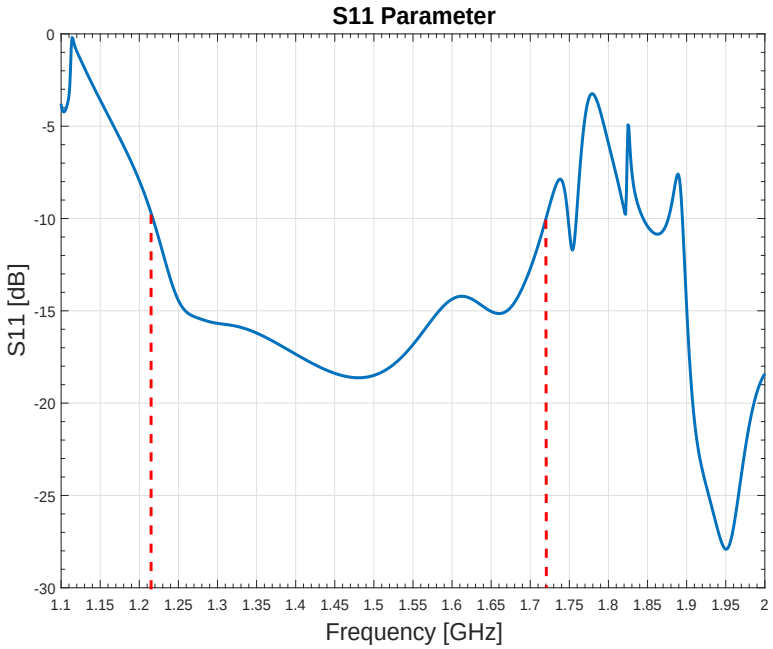

Figure 3.8: S11 Parameter

In the Figures 3.9, 3.10, 3.11 and 3.12 below, the radiation pattern of the antenna can be seen, at the central frequency 1.3 GHz and at edges of the band (1.21 GHz and 1.72 GHz). It must be considered that the polarization vector is on the y-axis. The E-plane is the YZ plane (θ variable and $\phi = 90°$) and its copolar component is θ and its crosspolar component is ϕ. The H-plane is the XZ plane (θ variable and $\phi = 0°$) and its copolar and crosspolar components are ϕ and θ, respectively.

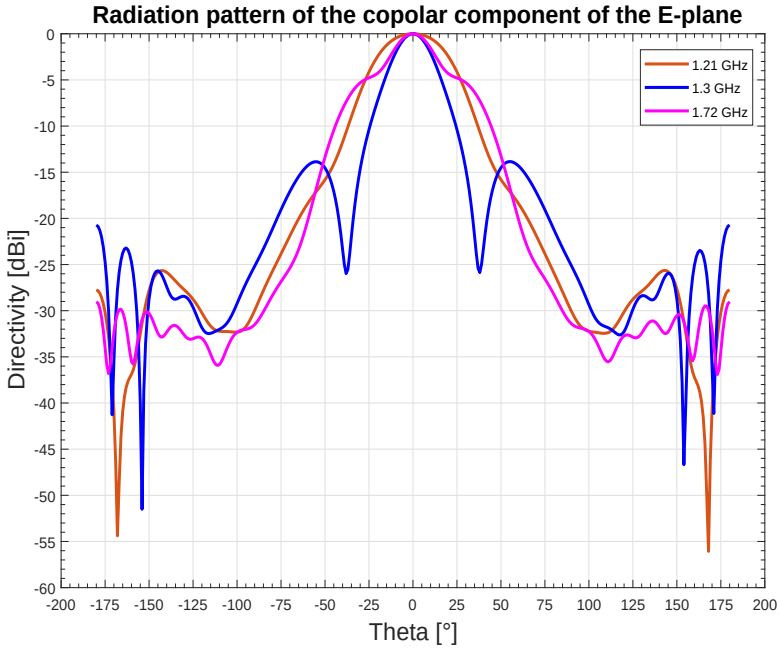

Figure 3.9: Radiation pattern of the copolar component of the E-plane

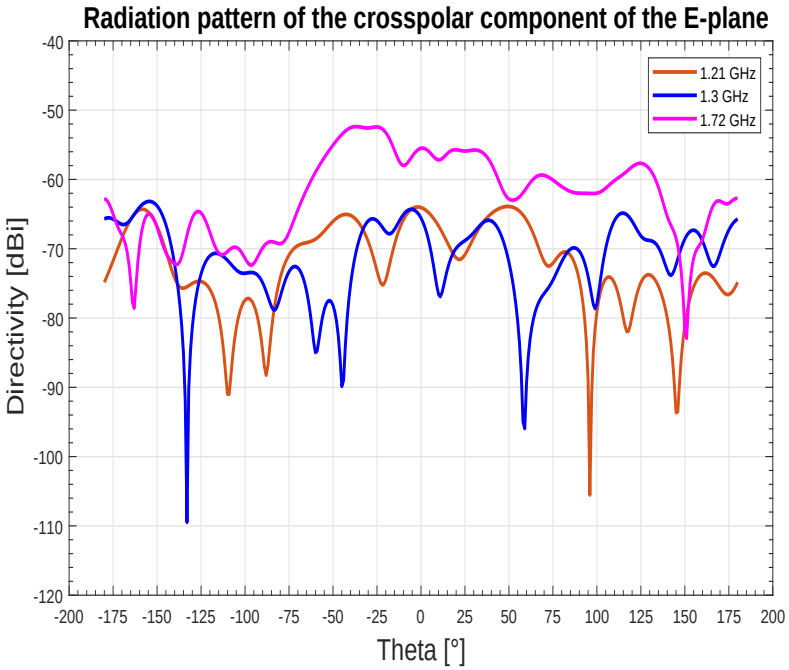

Figure 3.10: Radiation pattern of the crosspolar component of the E-plane

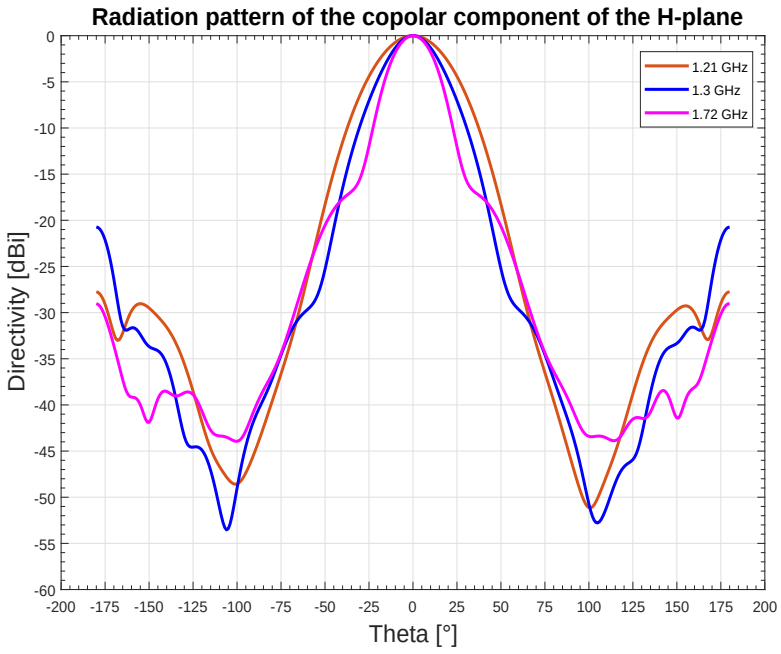

Figure 3.11: Radiation pattern of the copolar component of the H-plane

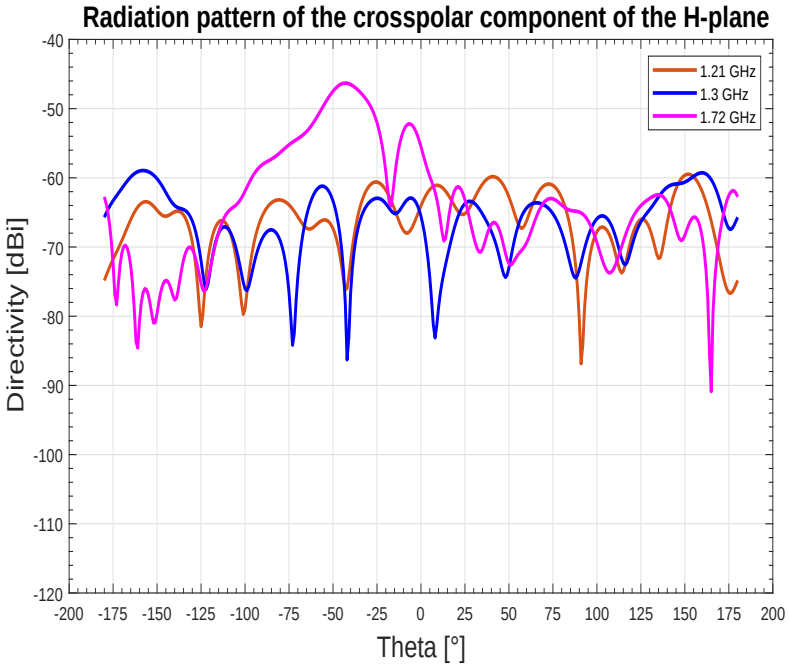

Figure 3.12: Radiation pattern of the crosspolar component of the H-plane

In Table 3.5 it can be seen the maximum gain, the side lobe level, the beamwidth at -3dB and at -10dB and the total efficiency of the antenna, at the central frequency and at the extreme frequencies.

Table 3.5: Antenna Characteristics

Frequency	**Maximum Gain[dBi]**	**Side Lobe Level[dB]**		**3-dB Beamwidth [°]**		**10-dB Beamwidth [°]**		**Total Efficiency**
		E-Plane	**H-Plane**	**E-Plane**	**H-plane**	**E-Plane**	**H-plane**	
1.21 GHz	13.32	-25.6	-27.7	43.7	41.2	73.70	74.75	88.31%
1.3 GHz	15.67	-13.8	-20.7	24.2	31	48.88	61.08	98.43%
1.72 GHz	14.75	-29	-29	29.3	25.6	88.55	45.42	91.76%

Second Genetic Algorithm Optimization

The first genetic algorithm may have failed because the search range was too wide. Following, a second optimization for the depth of the corrugations has been done, this time using a smaller range around the previously found values for each parameter. The obtained results can be found in Appendix 3, in Table 6. This time, the obtained gain is 15.62 dBi, higher than the gain obtained with the first genetic algorithm optimization.

In Figure 3.13 the reflection coefficient of the new system can be observed. The horn is matched between 1.2 GHz and 1.77 GHz and the bandwidth is approximately 576 MHz, higher than the bandwidth of the previous system. The radiation patterns for the central frequency and the extremes frequencies are shown in Figures 3.14, 3.15, 3.16 and 3.17. As it can be observed in Figure 3.14, the corrugations do not work anymore for the higher frequency.

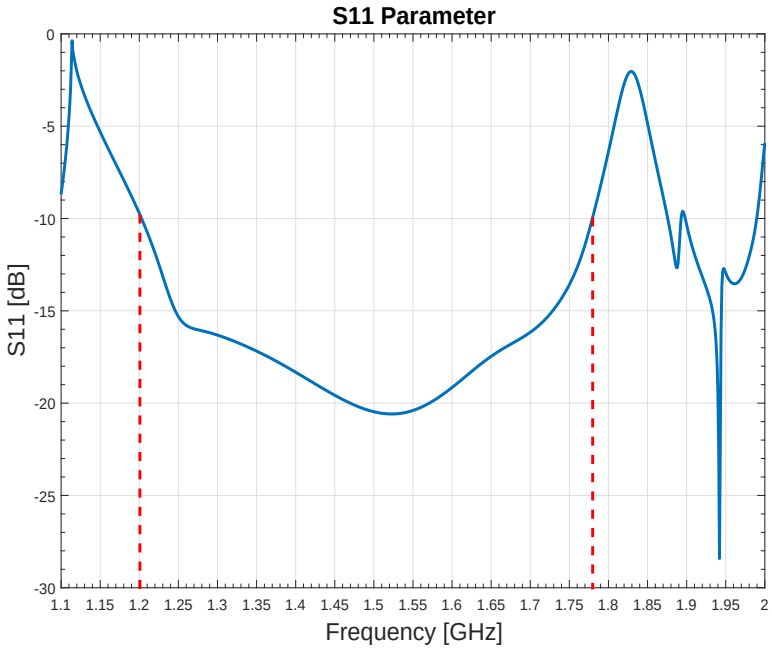

Figure 3.13: S11 Parameter

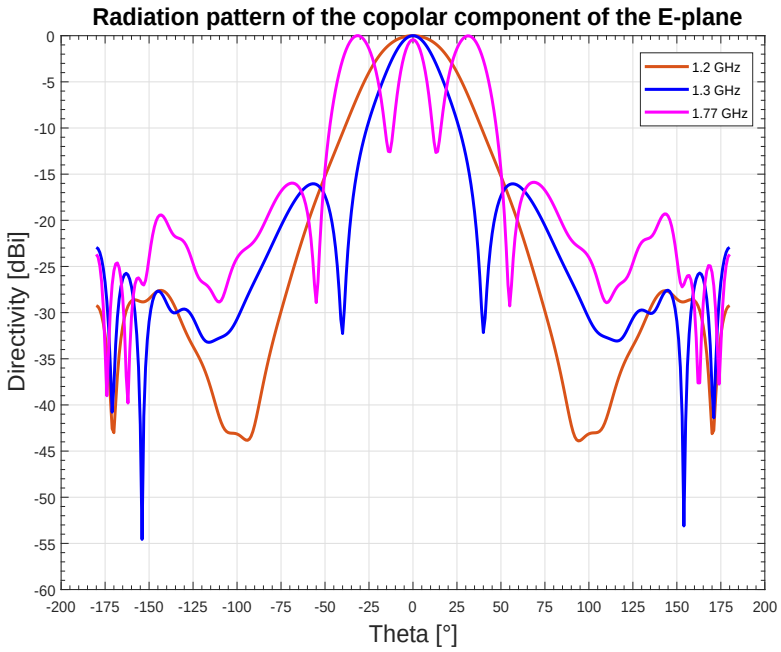

Figure 3.14: Radiation pattern of the copolar component of the E-plane

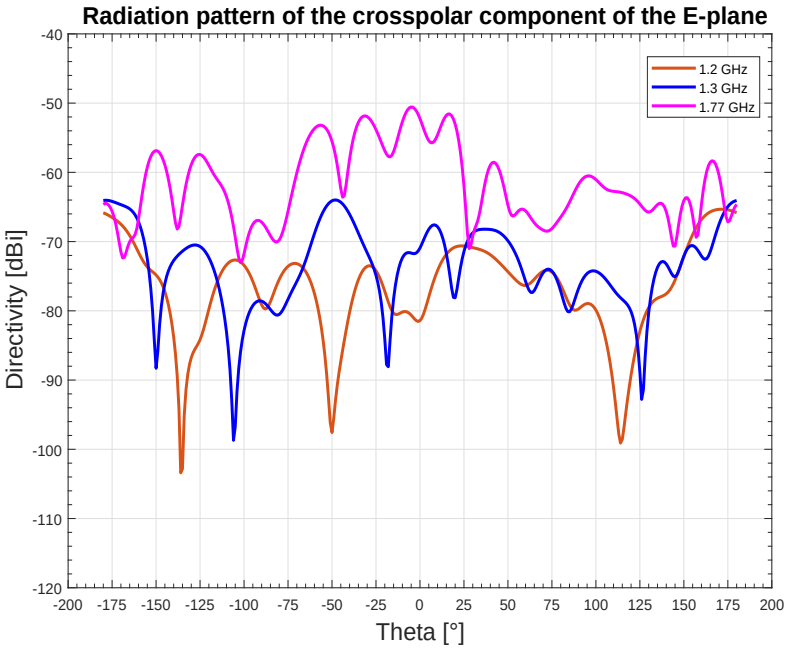

Figure 3.15: Radiation pattern of the crosspolar component of the E-plane

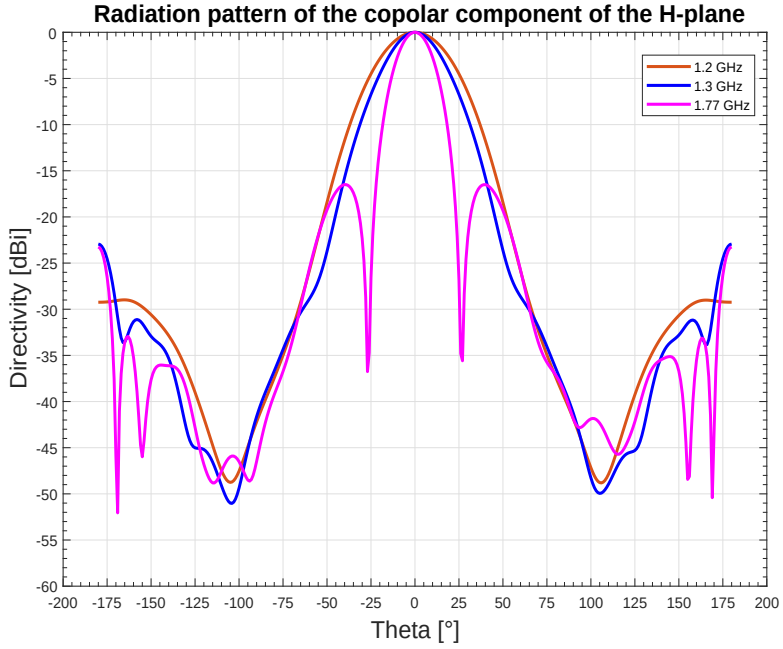

Figure 3.16: Radiation pattern of the copolar component of the H-plane

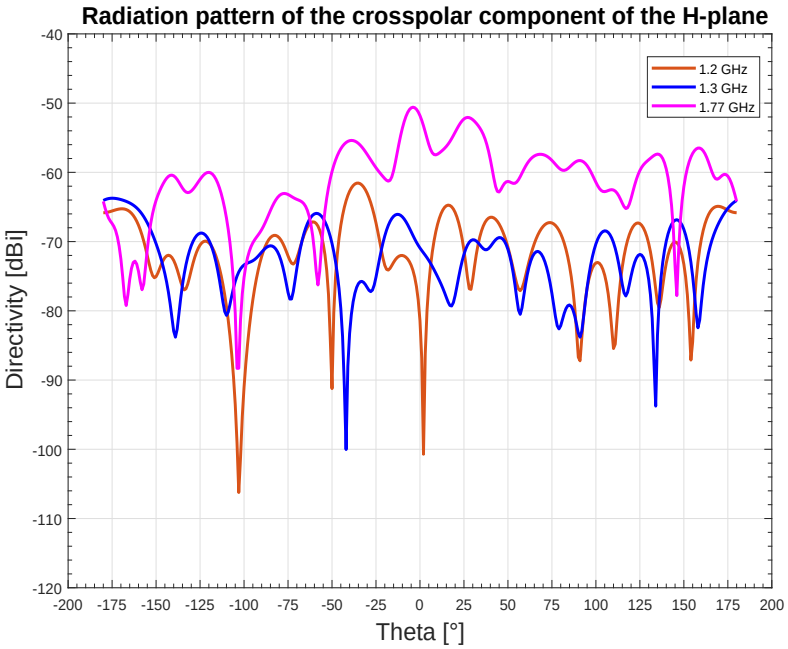

Figure 3.17: Radiation pattern of the crosspolar component of the H-plane

The maximum gain, the side lobe level, the beamwidth at -3dB and at -10dB and the total efficiency of the antenna at the central frequency and at the extreme frequencies are listed in Table 3.6.

Table 3.6: Antenna characteristics after optimization

Frequency	**Maximum Gain[dBi]**	**Side Lobe Level[dB]**		**3-dB Beamwidth [°]**		**10-dB Beamwidth [°]**		**Total Efficiency**
		E-Plane	**H-Plane**	**E-Plane**	**H-plane**	**E-Plane**	**H-plane**	
1.2 GHz	13.29	-27.6	-29	44.2	40.8	77.8	74	90.39%
1.3 GHz	15.62	-16	-22.9	26	31.9	52.4	62.6	99.01%
1.77 GHz	12.74	-15.9	-16.5	18.4	21	31.4	36.6	94.97%

In conclusion, after the optimization the gain variation is insignificant, as it decreased from 15.67 dBi to 15.62 dBi. On the other hand, for the central frequency, the side lobe levels in the E-plane and in the H-plane are lower and the efficiency is better, so from now on these depth values are going to be used in the next procedures.

3.3.2 Number of corrugations

The impact that the number of corrugations have on the horn is studied in this section. In order to achieve this aim, another two horns were designed: one with the minimmum number of corrugations: 10, and another one with more corrugations than the original one: 14.

10-Corrugations Horn

The dimensions of the corrugations have been calculated as shown in Appendix 3 in Table 7. The width and the teeth of the corrugations have the same values as in the previous system, since they are the maximum values that allow the correct functioning of the system. As a first approach, the depths are equal to the first 10 values found by the genetic algorithm.
Figure 3.18 shows the reflection coefficient S11. There is matching between 1.16 GHz and 1.75 GHz and the bandwidth is approximately **590 MHz**. The radiation patterns for the central frequency and the extremes frequencies are shown in Figures 3.19, 3.20, 3.21 and 3.22. In Figure 3.19 can be seen that the corrugations do not work for the highest frequency 1.75 GHz.

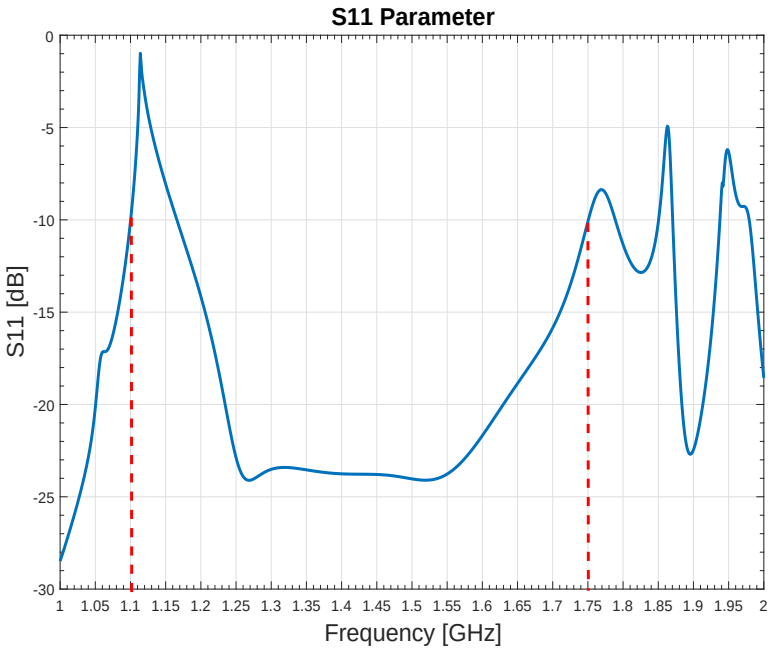

Figure 3.18: S11 Parameter

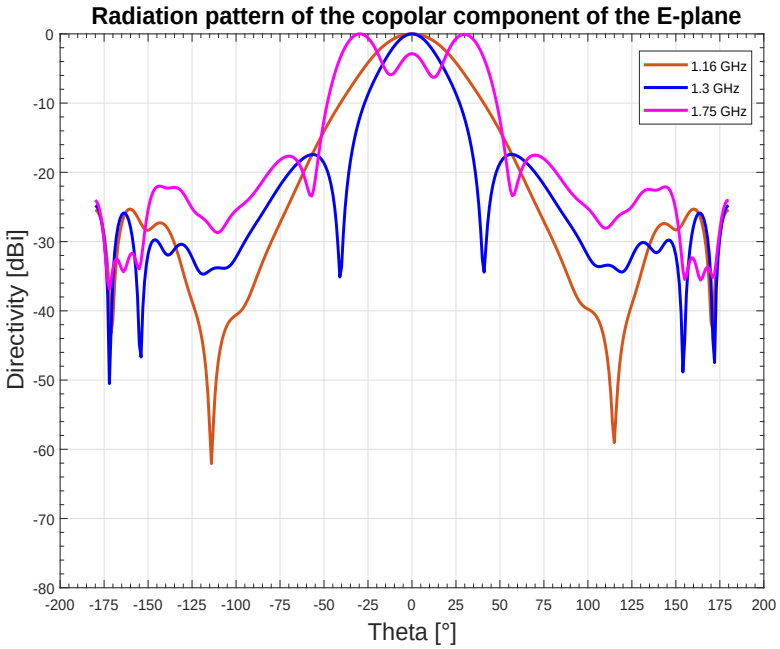

Figure 3.19: Radiation pattern of the copolar component of the E-plane

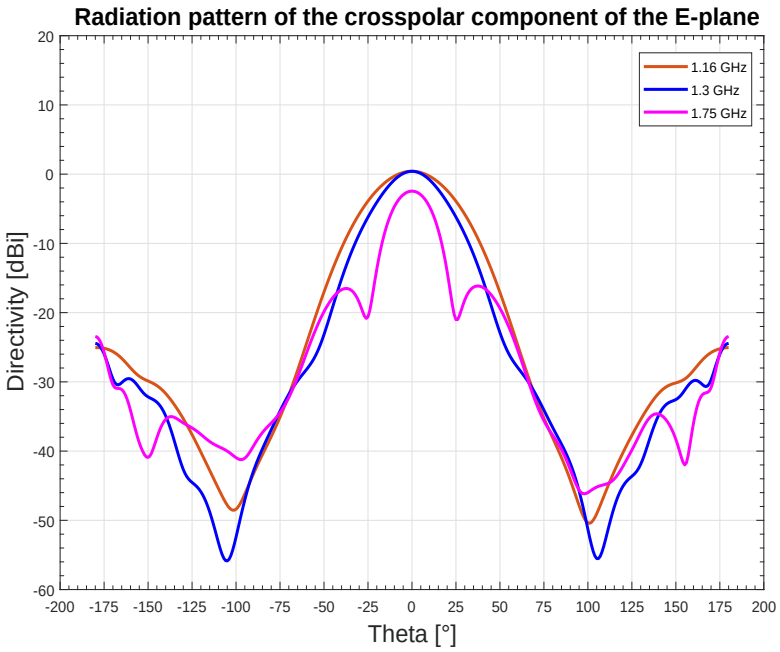

Figure 3.20: Radiation pattern of the crosspolar component of the E-plane

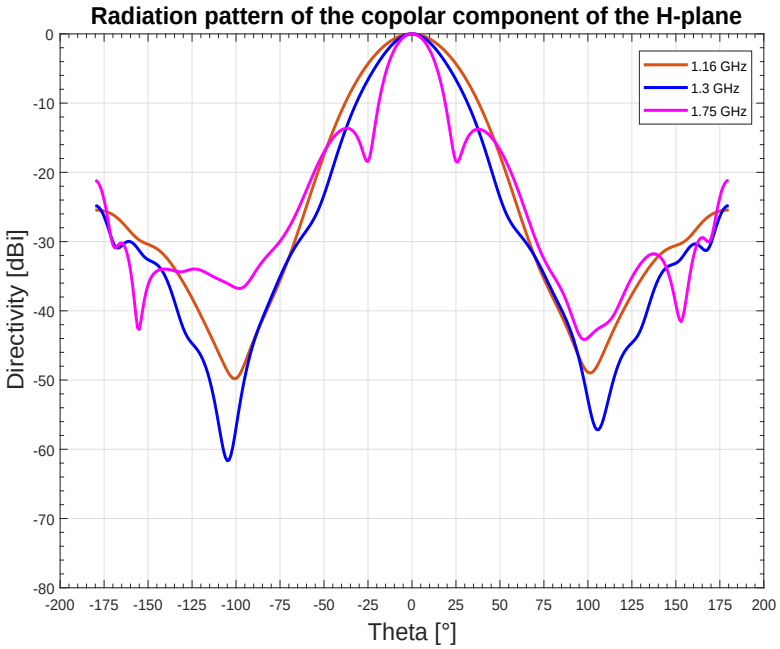

Figure 3.21: Radiation pattern of the copolar component of the H-plane

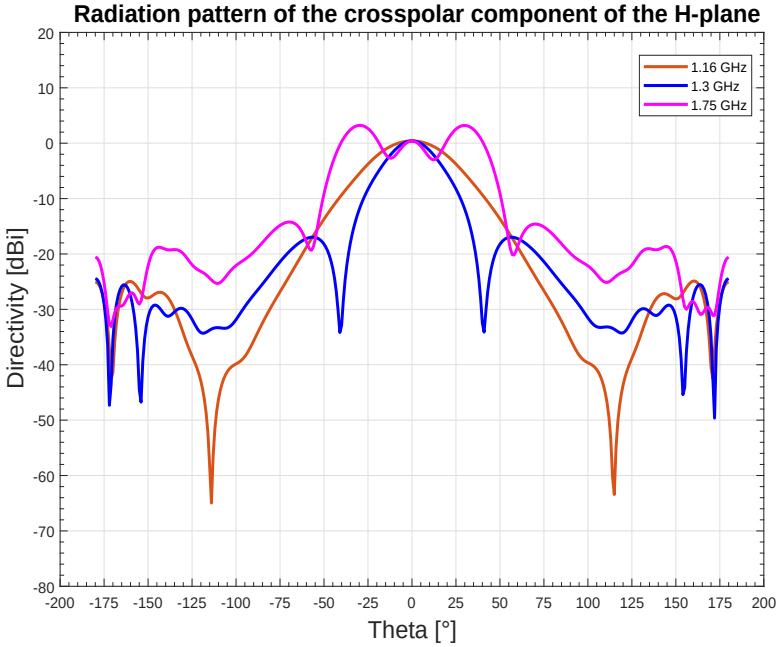

Figure 3.22: Radiation pattern of the crosspolar component of the H-plane

In Table 3.7 the maximum gain, the side lobe levels, the -3dB and -10dB Beamwidths and the total efficiency are shown for the central frequency and the lowest and the highest frequencies of the band:

Table 3.7: 10-corrugations horn characteristics before optimization

Frequency	Maximum Gain[dBi]	Side Lobe Level[dB]		3-dB Beamwidth [°]		10-dB Beamwidth [°]		Total Efficiency
		E-Plane	H-Plane	E-Plane	H-plane	E-Plane	H-plane	
1.16 GHz	13.19	-25.5	-25.5	42	41.9	78.4	78.5	89.57%
1.3 GHz	15.62	-20.1	-19.8	29.5	29.2	58.8	58.4	100%
1.75 GHz	12.75	-17.8	-17.3	22.4	22	96.56	97.1	93.52%

14-Corrugations Horn

The dimensions of the 14-corrugations horn are shown in Appendix 3 in Table 9. The width and the teeth of the corrugations are now lower, since the slant radius of the horn is the same and there are more corugations than previoulsy. The depths of the first ten corrugations have been equaled to the first ten optimized values found by the genetic algorithm for the 12-corrugations horn. For the last two corugations depths, another genetic algorithm optimization was performed, and values obtained are shown in the Table 9.
The reflection parameter S11 is shown in Figure 3.23, where can be seen that the horn is matched between 1.1 GHz and 1.72 GHz, obtaining a **620 MHz** bandwidth. In Figures 3.24, 3.25, 3.26 and 3.27 the radiation patterns of the E and H fields can be seen. The corrugations do not work for the highest frequency 1.72 GHz.

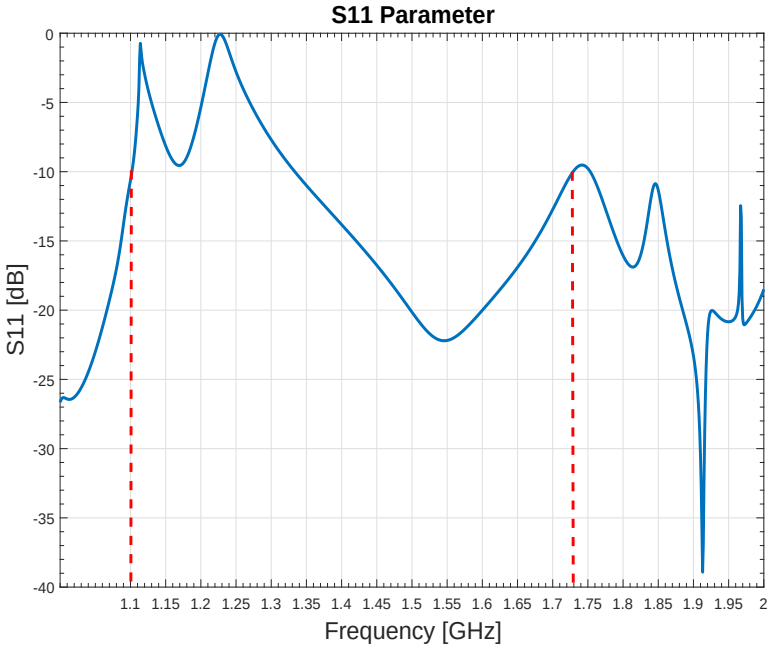

Figure 3.23: S11 Parameter

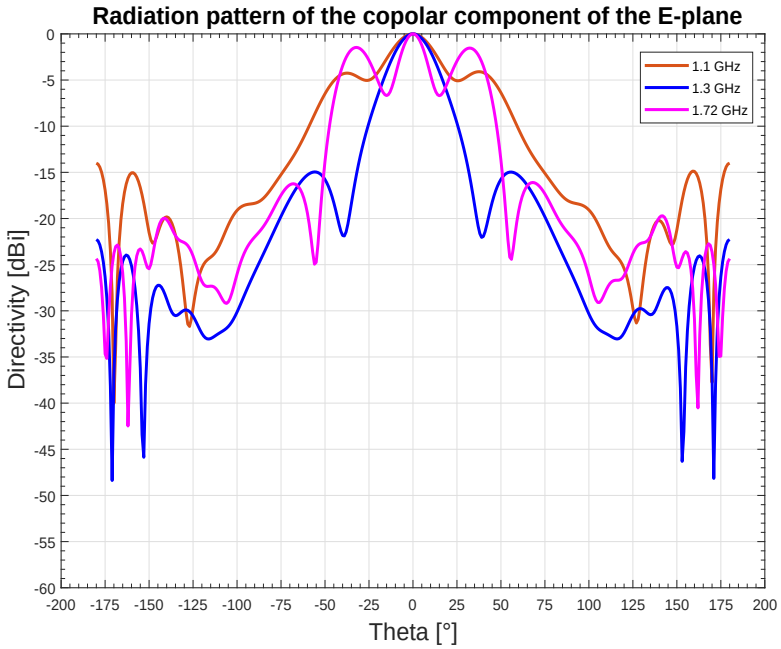

Figure 3.24: Radiation pattern of the copolar component of the E-plane

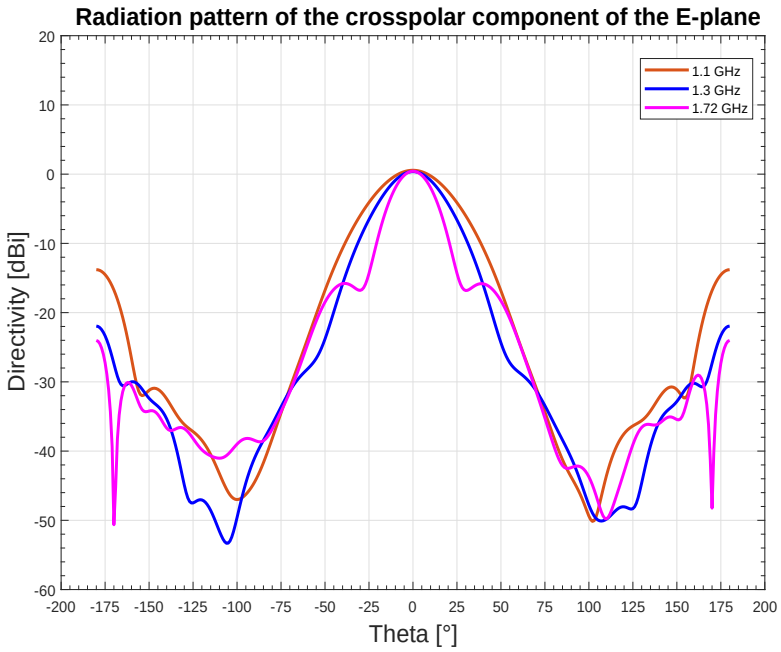

Figure 3.25: Radiation pattern of the crosspolar component of the E-plane

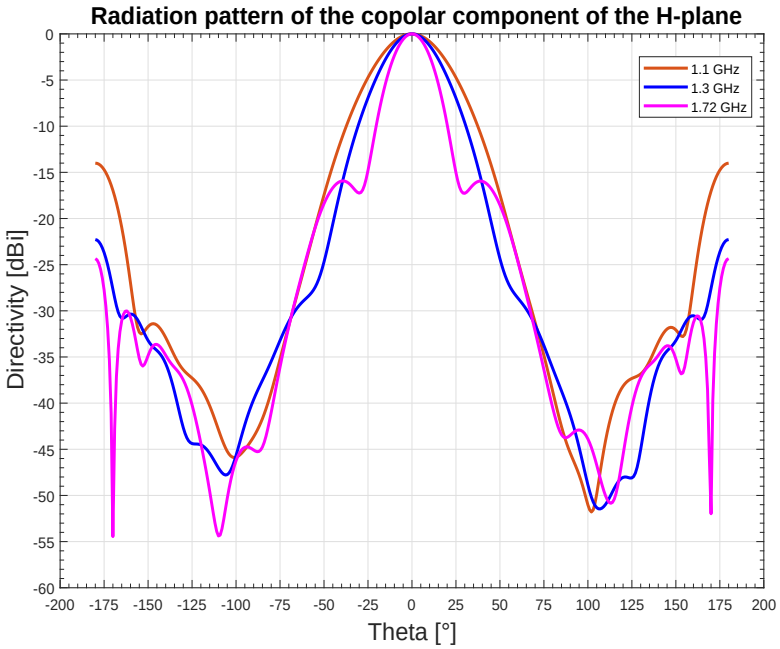

Figure 3.26: Radiation pattern of the copolar component of the H-plane

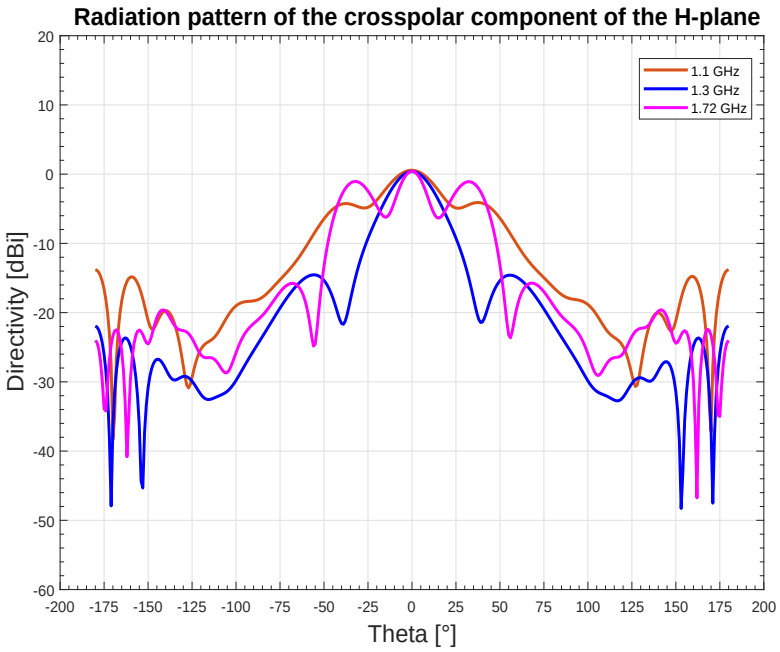

Figure 3.27: Radiation pattern of the crosspolar component of the H-plane

Table 3.8: 14-corrugations horn characteristics

Frequency	**Maximum Gain[dBi]**	**Side Lobe Level[dB]**		**3-dB Beamwidth [°]**		**10-dB Beamwidth [°]**		**Total Efficiency**
		E-Plane	**H-Plane**	**E-Plane**	**H-plane**	**E-Plane**	**H-plane**	
1.1 GHz	11.94	-14.2	-14.2	35.8	34.8	103.45	103.33	25.67%
1.3 GHz	15.68	-17.9	-17.5	28.3	28	56.82	56.40	85.05%
1.72 GHz	13.41	-4.6	-4.2	19.1	18.8	90.11	91.03	95.23%

In Table 3.8, the maximum gain, the side lobe levels, the -3dB and -10dB beamwidth in the E-plane and H-plane and the total efficiency are shown.

Conclusions

To observe the influence that the number of corrugations have on the total performance of the system, the maximum gain, the side lobe levels, the -3dB and -10dB beamwidth in the E-plane and H-plane and the total efficiency at the central frequency for the horns with 10, 12 and 14 corrugations are summarized in Table 3.9.

Table 3.9: Horns characteristics

Number of Corrugations	**Maximum Gain[dBi]**	**Side Lobe Level[dB]**		**3-dB Beamwidth [°]**		**10-dB Beamwidth [°]**		**Total Efficiency**
		E-Plane	**H-Plane**	**E-Plane**	**H-plane**	**E-Plane**	**H-plane**	
10	15.62	-20.1	-19.8	29.5	29.2	58.8	58.4	100%
12	15.62	-16	-22.9	26	31.9	52.4	62.6	99.01%
14	15.68	-17.9	-17.5	28.3	28	56.82	56.40	85.05%

As it can be observed in the table, the number of corrugations do not have a significant influence on the gain. Regarding the side lobe level, the horn with 10 corrugations has the lowest side lobe level in the E-plane, the highest -3dB and -10dB beamwidths in the E-plane and the best efficiency. The horn with 12 corrugations has the lowest side lobe level and the highest -3dB and -10dB beamwidths in the H-plane.

3.4 Array Design

In this section an array is generated with each type of horn: 10-corrugations horn, 12-corruagtions horn and 14-corrugations horn. For the first two horns, the optimized depths values were used, since they give a better performance to the system. The array is formed by four horns: two in y-axis and two in the z-axis. The elements must be placed side by side, so the distance between centers is the diameter of the aperture of the horn. First, the difference patterns of each array are shown, and then the sum patterns are compared with the TIRA sum patterns.

3.4.1 Array formed by four 10-corrugations horns

In the Figures below a comparison is made between the radiation patterns of the array formed by four 10-corrugations horns and the radiation patterns of the TIRA system, at the central frequency 1.3 GHz.

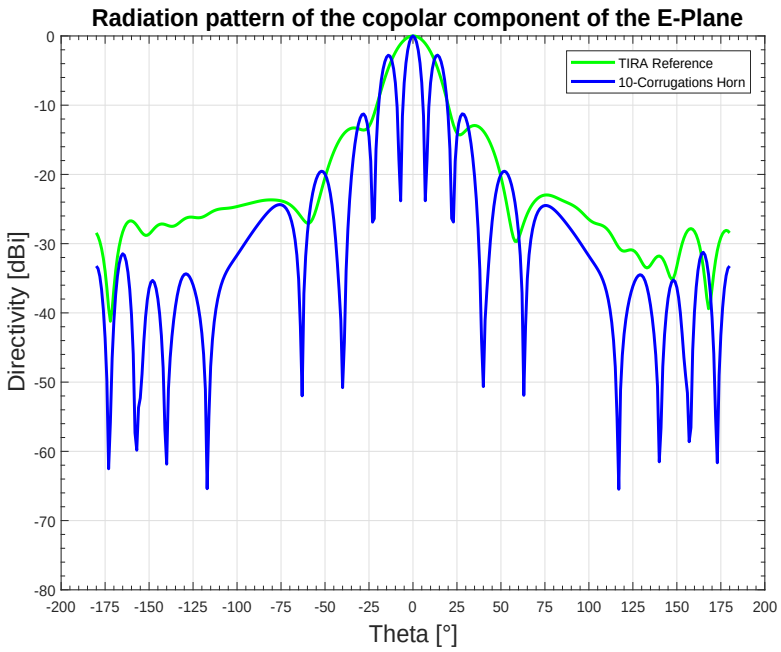

Figure 3.28: Radiation patterns of the copolar components of the E-plane of the horns array and the TIRA Reference

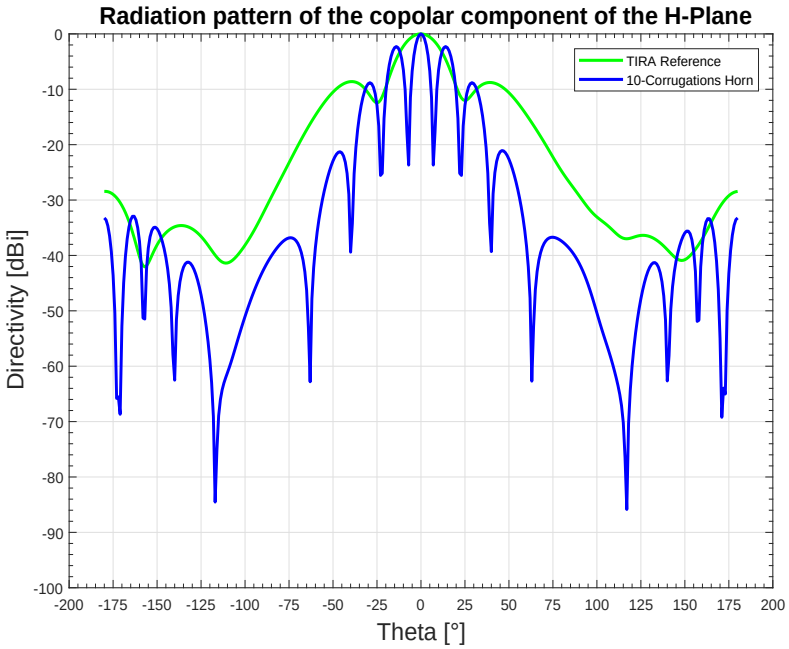

Figure 3.29: Radiation patterns of the copolar components of the H-plane of the horns array and the TIRA Reference

In Figures 3.28 and 3.29 can be observed that the radiation patterns of the corrugated horn have more lobes than the TIRA reference. Some of them are visibly lower than the side lobes of the TIRA reference, and others are at the same level or higher. The radiation pattern has a zero in 40°, where the side lobe of the TIRA pattern is located.

3.4.2 Array formed by four 12-corrugations horns

In the Figures below a comparison is made between the radiation patterns of the array formed by four 12-corrugations horns and the radiation patterns of the TIRA system, at the central frequency 1.3 GHz.

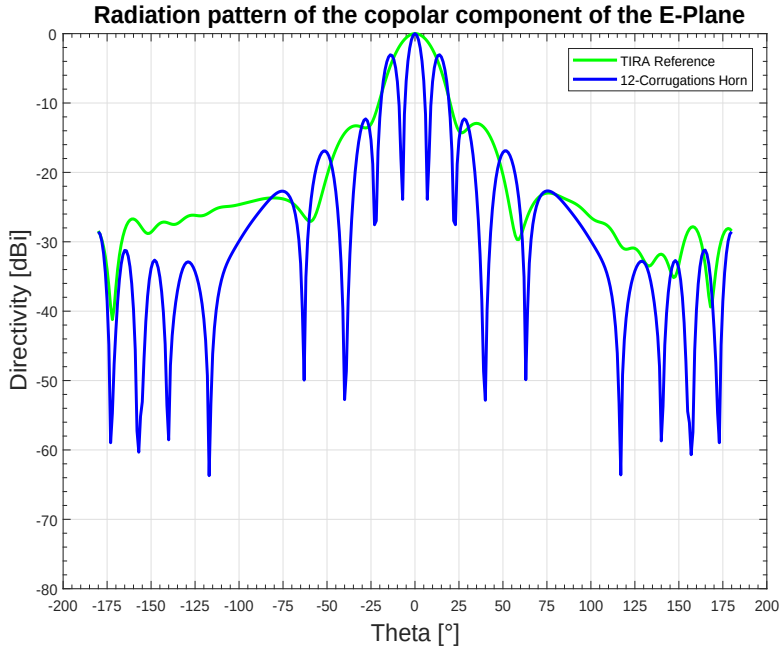

Figure 3.30: Radiation pattern of the copolar components of the E-plane of the horns array and the TIRA Reference

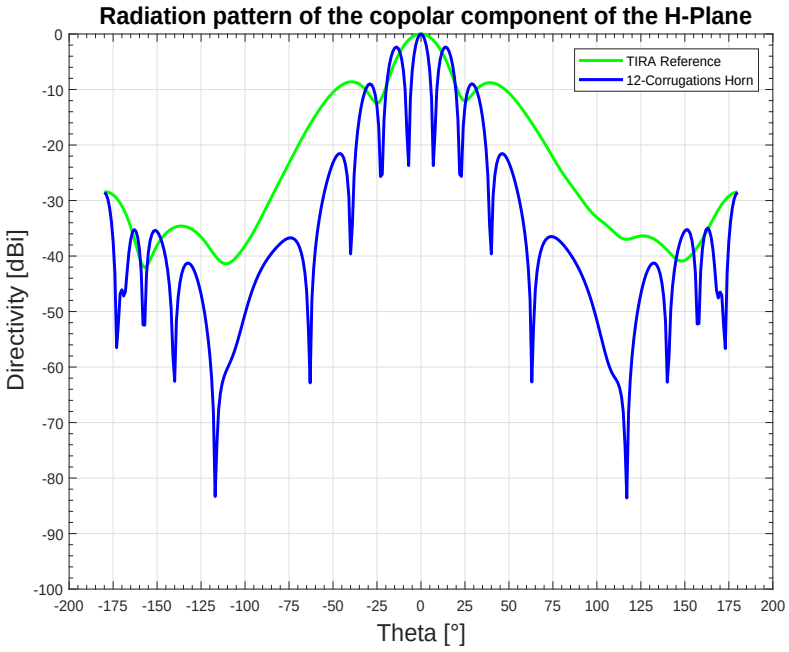

Figure 3.31: Radiation patterns of the copolar components of the H-plane of the horns array and the TIRA Reference

In Figures 3.30 and 3.31 can be observed that some lobes of the 12-corrugations horn are lower than the side lobes of the TIRA reference. Comparing with the radiation pattern of the 10-corrugations horn, the side lobes are higher.

3.4.3 Array formed by four 14-corrugations horns

In the Figures below a comparison is made between the radiation patterns of the array formed by four 14-corrugations horns and the radiation patterns of the TIRA system, at the central frequency 1.3 GHz.

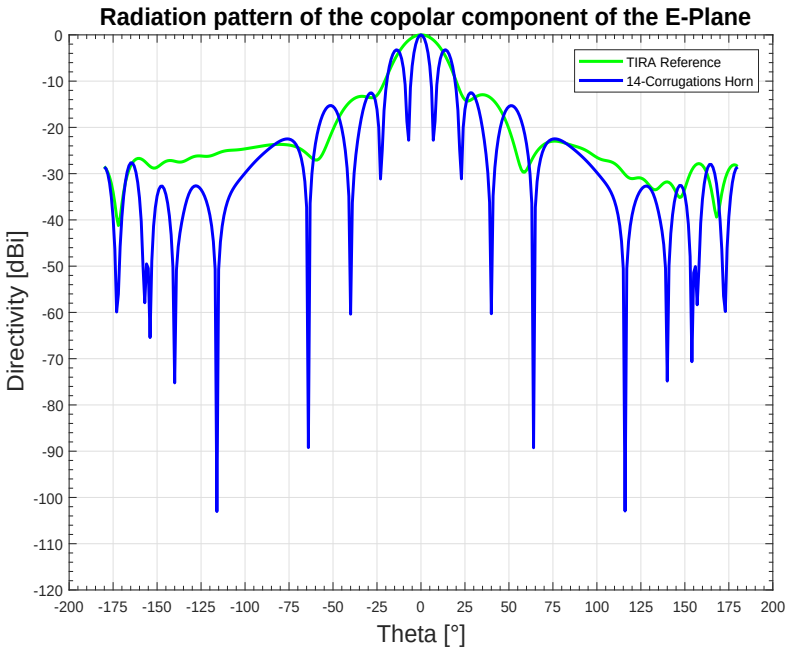

Figure 3.32: Radiation patterns of the copolar component of the E-plane of the horns array and the TIRA Reference

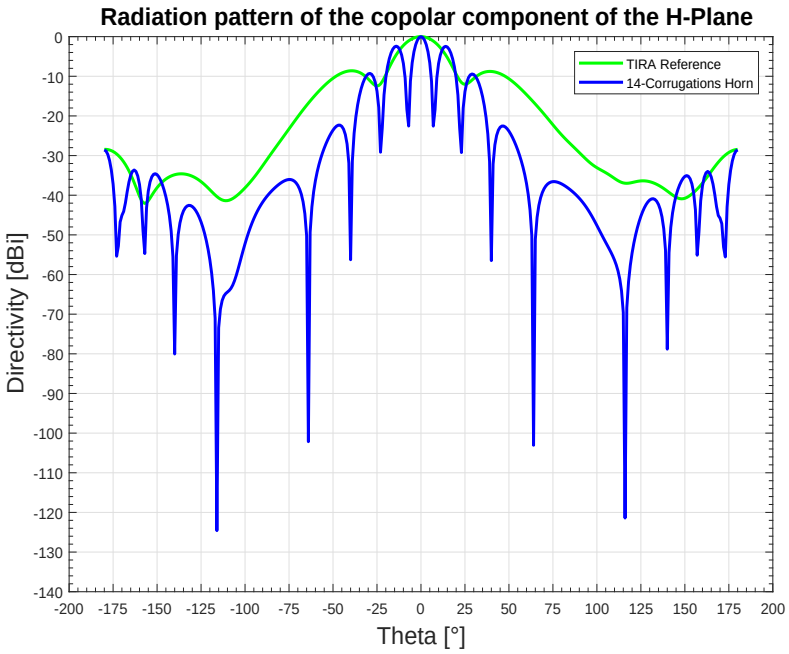

Figure 3.33: Radiation patterns of the copolar components of the H-plane of the horns array and the TIRA Reference

In Figures 3.32 and 3.33 can be observed that the side lobe levels of the 14-corrugations horn are not lower than the side lobes of the TIRA radiation pattern.

4

Conclusions

In conclusion, it was observed that the depth of the corrugations have a great effect on the system performance. The depth of a single corrugation can increase and decrease the gain or the beamwidth and therefore the side lobe level. The number of corrugations do not affect the gain of the antenna, but less corrugations provide a better performance of the system.

Regarding the horns arrays, grating lobes were observed in the radiation patterns, as the distance between elements is greater than λ_0. The main goal of this thesis was to achieve lower side lobes than the TIRA radiation pattern, and it was observed that with an array formed by four horns with ten corrugations, lower side lobes can be reached.

To fully demonstrate that the corrugated horns array is better than the smooth-wall horns array, some of the next steps would be: match the zero beamwidth to the reflector system, estimate the monopulse parameters and estimate safety limits.

Bibliography

[1] Fraunhofer Institute.
www.fhr.fraunhofer.de/en/the-institute/technical-equipment/space-observation-radar-tira.html.

[2] Merril I. Skolnik. Introduction to radar systems. pages 152–167, 2001.

[3] A. I. Leonov and K. I. Fomichev. Monopulse radar. pages 1–80, 1971.

[4] Ninoslav Majurec Davor Bonefacic, Julijana Jancula. Model of a monopulse radar tracking system for student laboratory. *Radioengineering, VOL 16, NO. 3*, pages 62–67, 2007.

[5] Dennis Kazakoff. Aperture antennas. *Antenna Theory and Applications*, pages 153–188, 2012.

[6] J. L. Masa Campos. Concepto antenas de apertura y antenas de bocina. pages 1–58, 2017.

[7] Constantine A. Balanis. Antenna theory. pages 783–791, 2005.

[8] Thomas A. Milligan. Modern antenna design. pages 336–379, 2005.

Appendix 1: Corrugations Coordinate System

To calculate the coordinates of the corrugations it is important to consider β, the angle between the center of the axis and the top of the corrugations, showed in Figure 1.

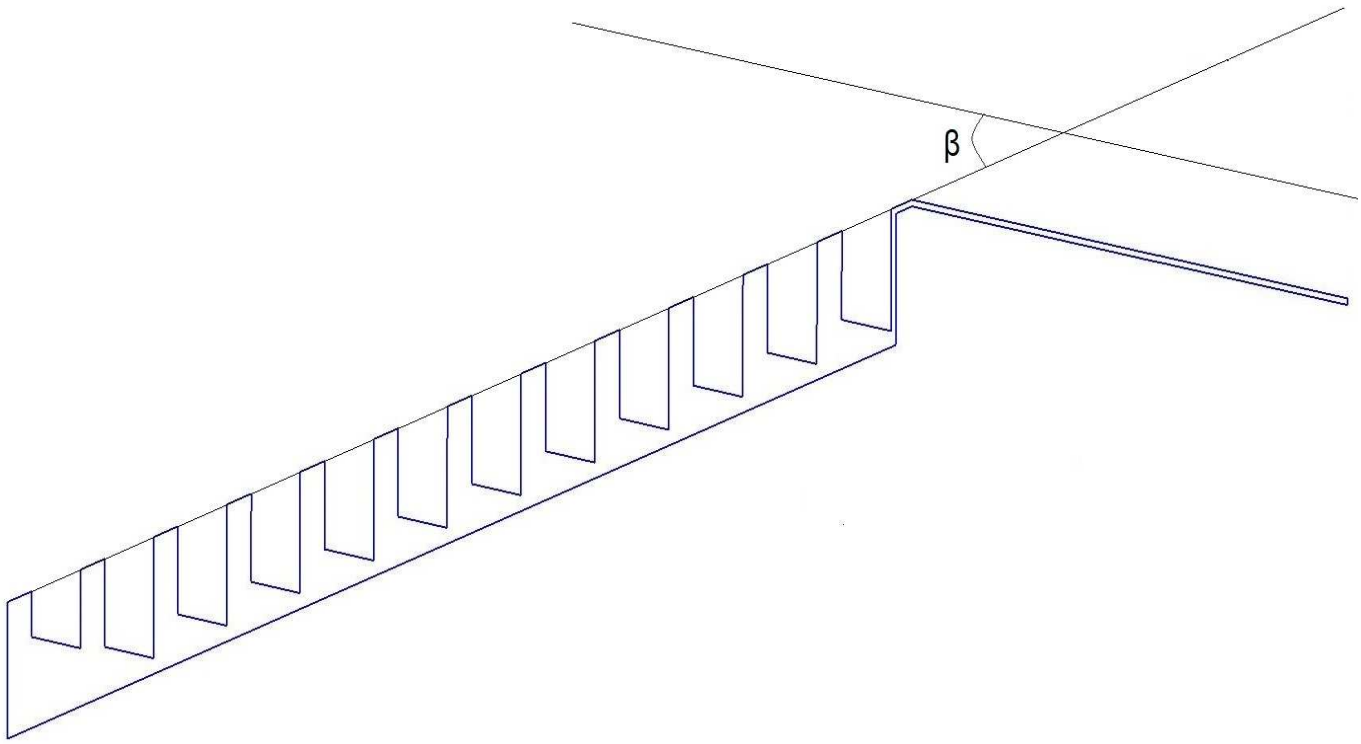

Figure 1: Cross section of the horn

Applying alternate angles it is possible to calculate the coordinate of each point of the corrugations. In Figure 2 it is illustrated how the coordinates starting from the aperture have been calculated. It must be considered that t_1 and t_2 represent the teeths of the first and second corrugation, w_1 is the width of the first corrugation and D_1 and D_2 are the depths of the first and second corrugation, respectively.

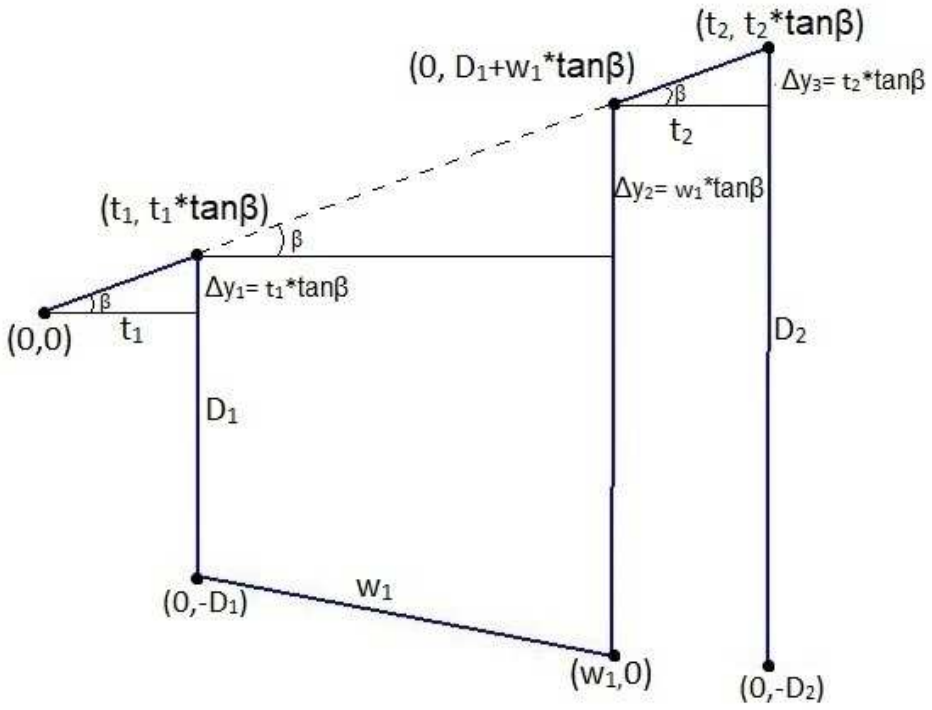

Figure 2: Coordinates of the first two corrugations.

The coordinates of the rest of the corrugations have been calculated in the same way. They are listed in Table 1 and shown in Figure 3.

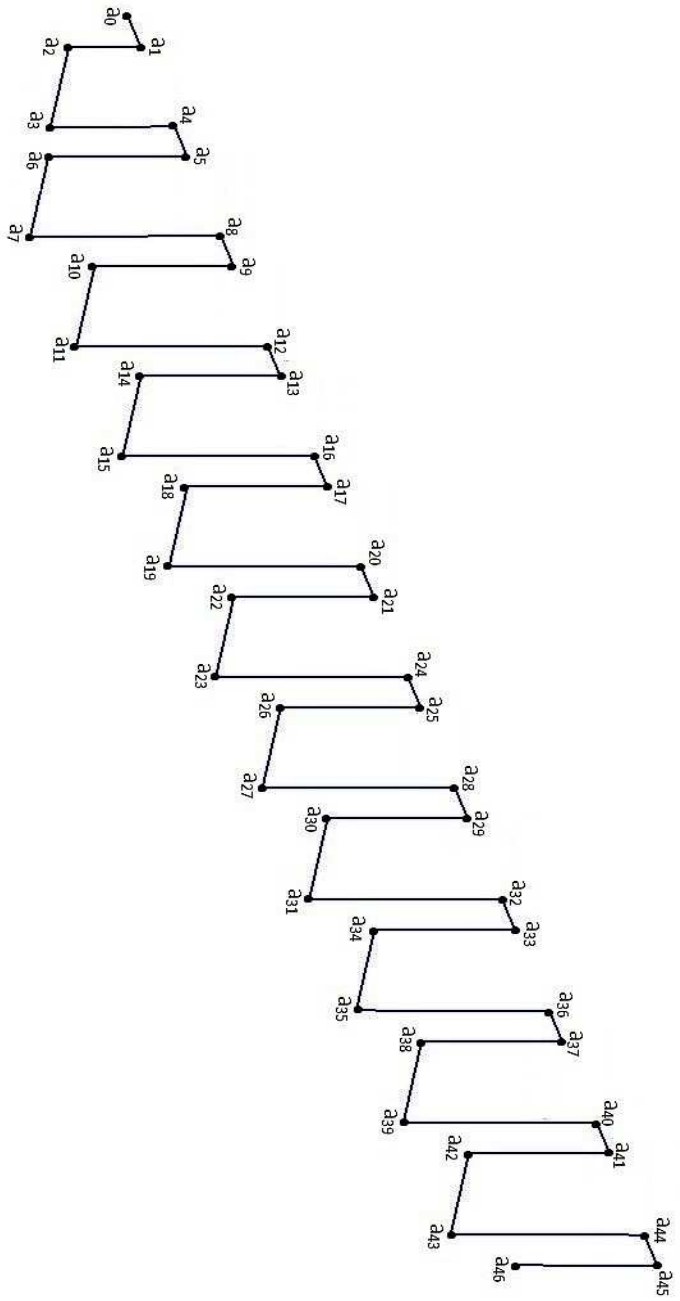

Figure 3: Coordinates defined by points

Table 1: Coordinates of the 12 corrugations

Point	**Coordinates**	
	X	**Y**
a_0	0	0
a_1	t_1	$t_1 \tan\beta$
a_2	0	-D_1
a_3	w_1	0
a_4	0	$D_1 + w_1 \tan\beta$
a_5	t_2	$t_2 \tan\beta$
a_6	0	-D_2
a_7	w_2	0
a_8	0	$D_2 + w_2 \tan\beta$
a_9	t_3	$t_3 \tan\beta$
a_{10}	0	-D_3
a_{11}	w_3	0
a_{12}	0	$D_3 + w_3 \tan\beta$
a_{13}	t_4	$t_4 \tan\beta$
a_{14}	0	-D_4
a_{15}	w_4	0
a_{16}	0	$D_4 + w_4 \tan\beta$
a_{17}	t_5	$t_5 \tan\beta$
a_{18}	0	-D_5
a_{19}	w_5	0
a_{20}	0	$D_5 + w_5 \tan\beta$
a_{21}	t_6	$t_6 \tan\beta$
a_{44}	0	$D_{11} + w_{11} \tan\beta$
a_{46}	0	-D_{12}

Point	**Coordinates**	
	X	**Y**
a_{22}	0	-D_6
a_{23}	w_6	0
a_{24}	0	$D_6 + w_6 \tan\beta$
a_{25}	t_7	$t_7 \tan\beta$
a_{26}	0	-D_7
a_{27}	w_7	0
a_{28}	0	$D_7 + w_7 \tan\beta$
a_{29}	t_8	$t_8 \tan\beta$
a_{30}	0	-D_8
a_{31}	w_8	0
a_{32}	0	$D_8 + w_8 \tan\beta$
a_{33}	t_9	$t_9 \tan\beta$
a_{34}	0	-D_9
a_{35}	w_9	0
a_{36}	0	$D_9 + w_9 \tan\beta$
a_{37}	t_{10}	$t_{10} \tan\beta$
a_{38}	0	-D_{10}
a_{39}	w_{10}	0
a_{40}	0	$D_{10} + w_{10} \tan\beta$
a_{41}	t_{11}	$t_{11} \tan\beta$
a_{42}	0	-D_{11}
a_{43}	w_{11}	0
a_{45}	t_{12}	$t_{12} \tan\beta$

Then, the waveguide has been built considering that there must be a small distance between it and the last corrugation. First, a line which represents the length of the waveguide has been added(Figure 4a) and in order to give thickness to the horn the curve has been closed starting by the end point of this line(Figure 4b). Finally, for the aperture of the waveguide, a circle whose radius is the radius of the waveguide has been attached at the end of the curve(Figure 3c). In Figure 3, the coordinates of the points generated for each step mentioned above can be seen.

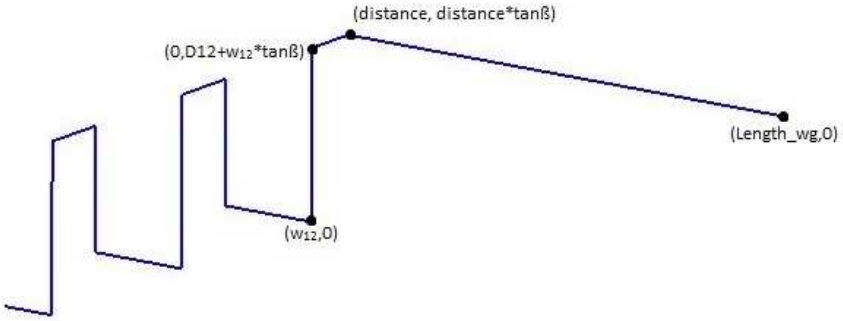

(a) Step 1: Coordinates of the points which form the waveguide length

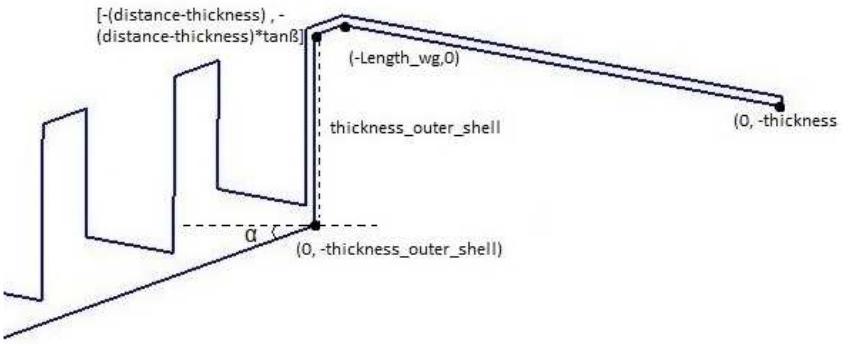

(b) Step 2: Coordinates of the points which close the curve

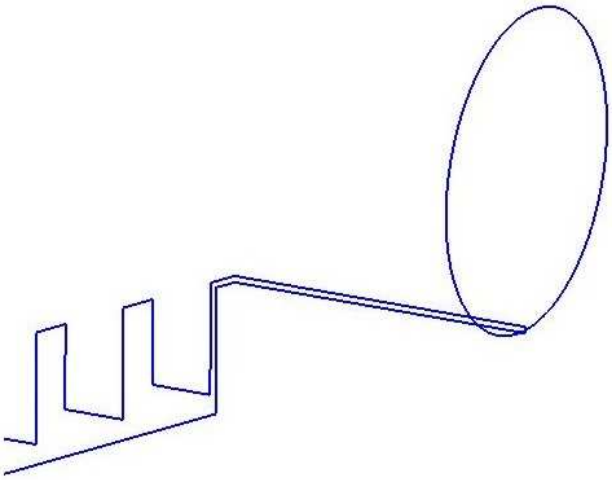

(c) Step 3: Aperture of the waveguide

Figure 3: Cross section of the waveguide

For closing the curve two new parameters have been defined: the *thickness outer shell* and the angle α. The *thickness_outer_shell* is the length of the line parallel to the depth of the corrugations, while α is the angle between the line perpendicular to the latter one and the exterior line at the bottom of the corrugations. Their values are shown in Table 2. In Figure 4 the coordinates of the last point used for closing the curve can be seen.

Table 2: Auxiliary parameters

Parameter	**Value**	**Units**
thickness_outer_shell	120	*mm*
α	0.69	*rad*

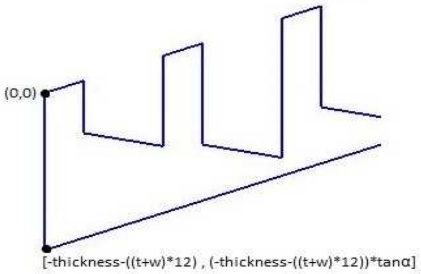

Figure 4: Cross section of the aperture of the horn

Appendix 2: Step-by-step tuning

Second Corrugation Depth

A parameter sweep for the depth of the second corrugation has been done to figure out which depth leads to the maximum gain. Its effects on the gain and on the beamwidth can be observed in the figures below:

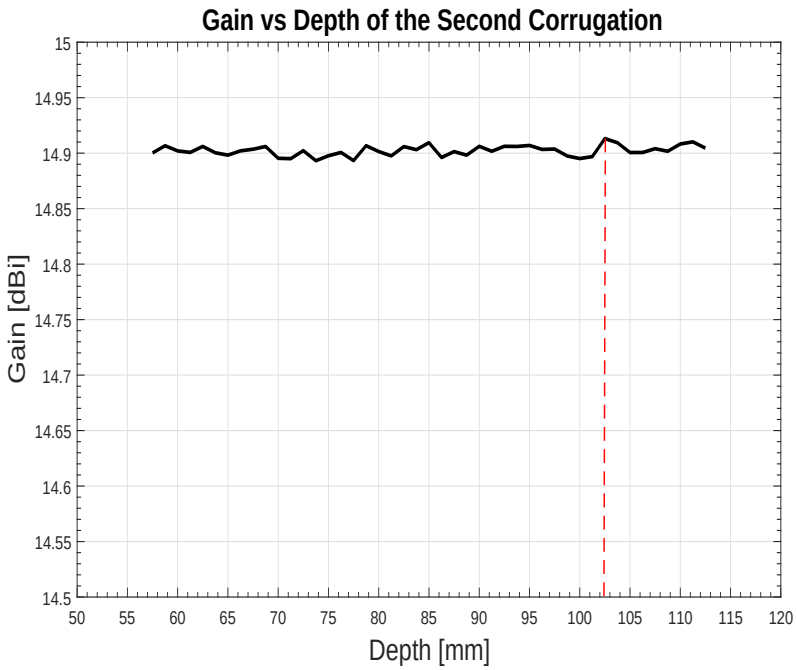

Figure 5: Gain vs Depth of the second corrugation

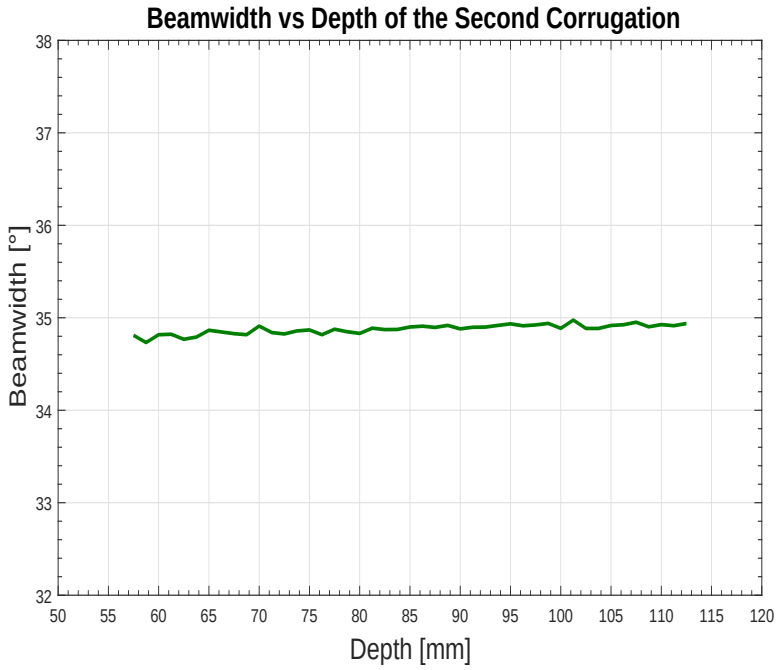

Figure 6: 3-dB Beamwidth vs Depth of the the second corrugation

The Figure 5 shows how the gain of the antenna varies as the depth of the second corrugation increases. As the red line marks, the higher gain that can be obtained is 14.9132 dBi for a 102.5 mm depth. In the Figure 6 is represented how the 3-dB beamwidth changes when the depth of the second corrugation increases. As it can be observed, the beamwidth variation respect to the depth is not significant. For a 102.5 mm depth, the beamwidth value is 34.88°.

Third Corrugation Depth

Previously it was demonstrated that a 102.5 mm second corrugation depth enhances the gain. Now is studied for which third corrugation depth, a higher gain can be obtained.

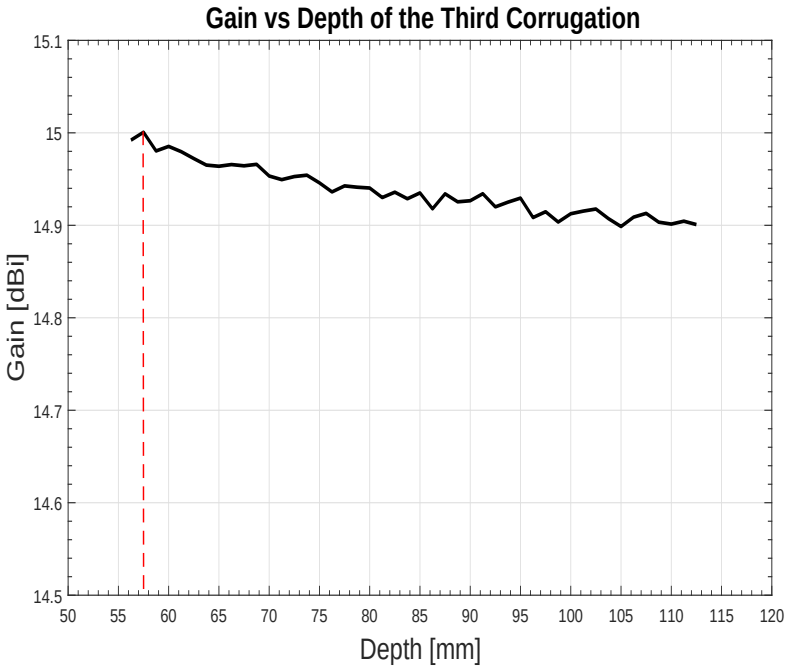

Figure 7: Gain vs Depth of the third corrugation

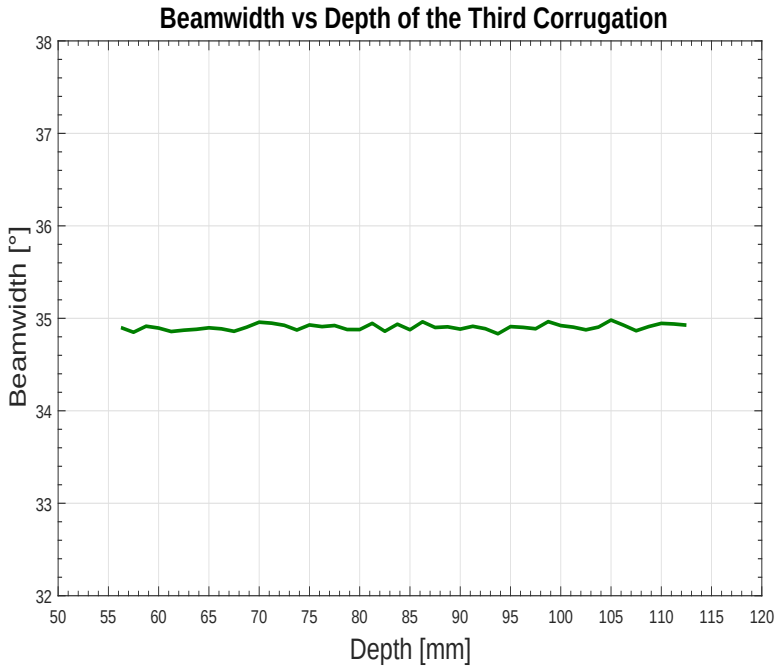

Figure 8: 3-dB Beamwidth vs Depth of the third corrugation

As the red line indicates in Figure 7, the highest gain obtained is 15 dB for a 57.5 mm depth. Figure 8 shows that the beamwidth variation is not significant and for a 57.5 mm depth, the beamwidth is 34.85°.

Fourth Corrugation Depth

Another simulation has been performed in order to find out the depth of the fourth corrugation which maximizes the gain.

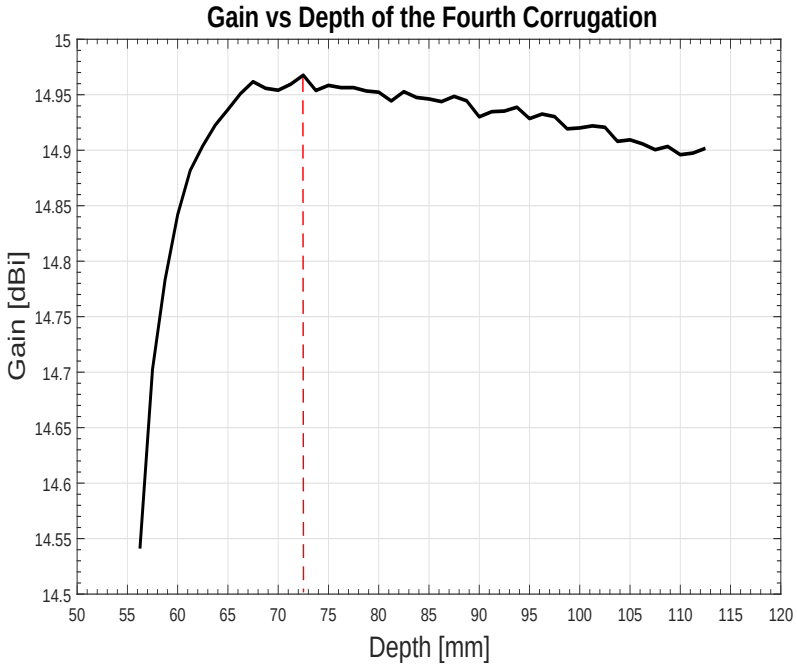

Figure 9: Gain vs Depth of the fourth corrugation

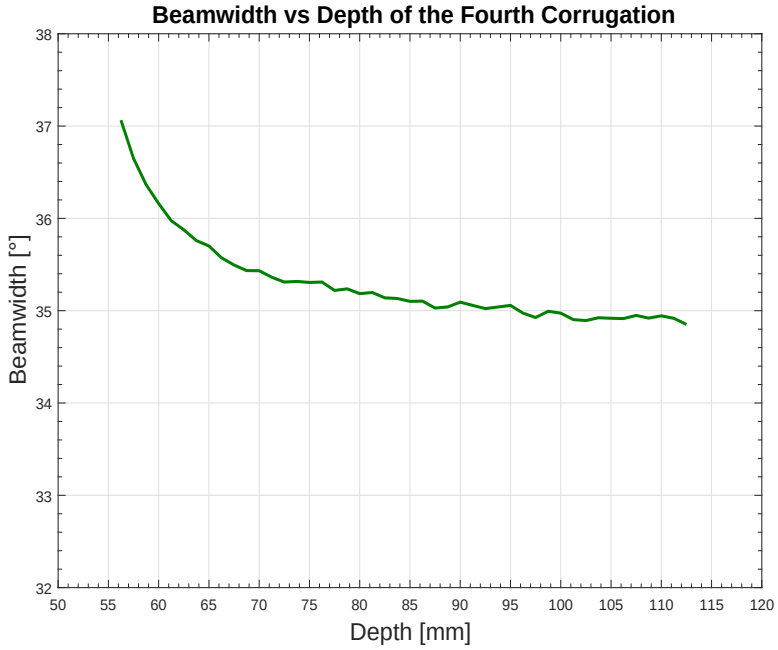

Figure 10: 3-dB Beamwidth vs Depth of the fourth corrugation

Figure 9 shows that the maximum gain obtained is 14.96 dB for 72.5 mm depth. Respecting the beamwidth, this time it can be observed from Figure 10 that the beamwidth decreases as the depth increments. For 72.5 mm depth, the beamwidth is 35.31°.

Fifth Corrugation Depth

At the beginning, the first corrugation's depth was fixed to 56.25 mm and the rest to 108 mm. A parameter sweep from $\frac{\lambda_0}{4} = 56.25$ mm to $\frac{\lambda_0}{2} = 112.5$ mm was done in a parallel way for the second, third and fourth corrugations. To see if the total gain of the antenna has improved, the next simulations are performed with the best depth values found for the first four corrugations. The depth values used in this simulations are showed in Table 3. A parameter sweep from $\frac{\lambda_0}{4}$ to $\frac{\lambda_0}{2}$ have been performed for the depth of the fifth corrugation to find out which value gives the best gain.

Table 3: Depth values for the simulation

Parameter	**Symbol**	**Value**	**Units**
Depth of the first corrugation	D_1	56.25	mm
Depth of the second corrugation	D_2	102.5	mm
Depth of the third corrugation	D_3	57.5	mm
Depth of the fourth corrugation	D_4	72.5	mm
Depth of the sixth corrugation	D_6	108	mm
Depth of the seventh corrugation	D_7	108	mm
Depth of the eighth corrugation	D_8	108	mm
Depth of the ninth corrugation	D_9	108	mm
Depth of the tenth corrugation	D_{10}	108	mm
Depth of the eleventh corrugation	D_{11}	108	mm
Depth of the twelfth corrugation	D_{12}	108	mm

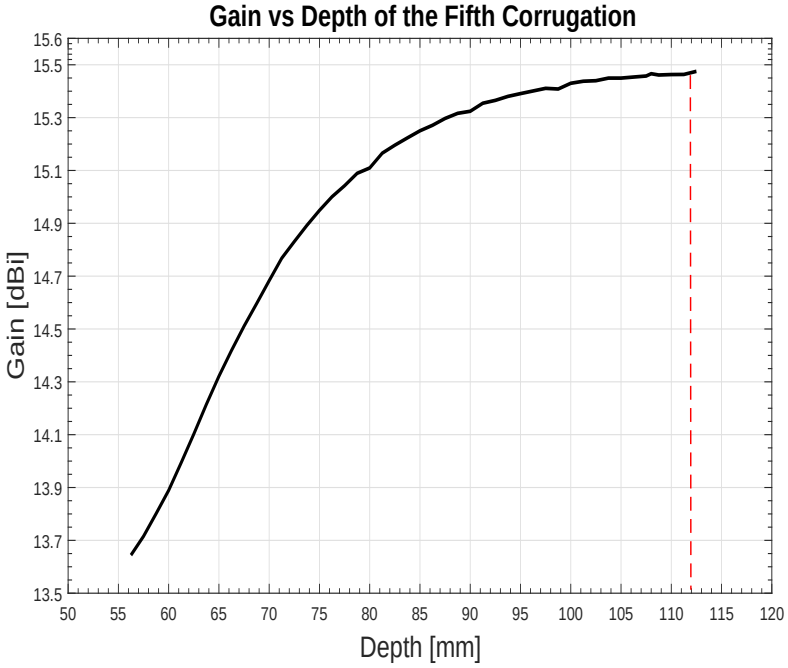

Figure 11: Gain vs Depth of the fifth corrugation

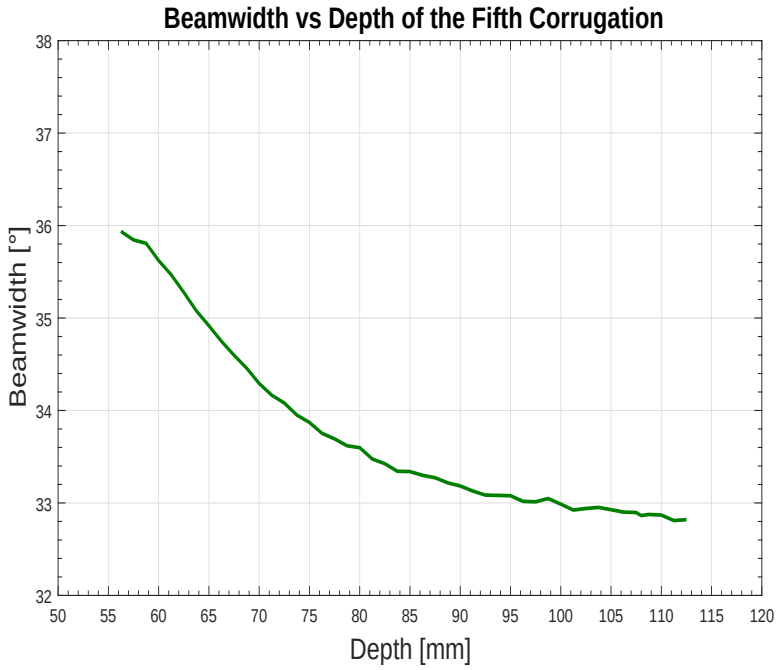

Figure 12: 3-dB Beamwidth vs Depth of the fifth corrugation

As it can be observed in Figure 11, the gain increases when the depth is getting closer to $\frac{\lambda}{2} = 112.5$ mm and maximum gain obtained is 15.475 dBi. Therefore, a depth value close to a half-wavelength was choosen: 112 mm. In Figure 12 it can be observed that the beamwidth decreases while the depth increments. For 112 mm depth, the beamwidth is approximately 32.93°.

Sixth Corrugation Depth

This time a parameter sweep for the depth of the sixth corrugation from $\frac{\lambda_0}{4}$ to $\frac{\lambda_0}{2}$ has been performed.

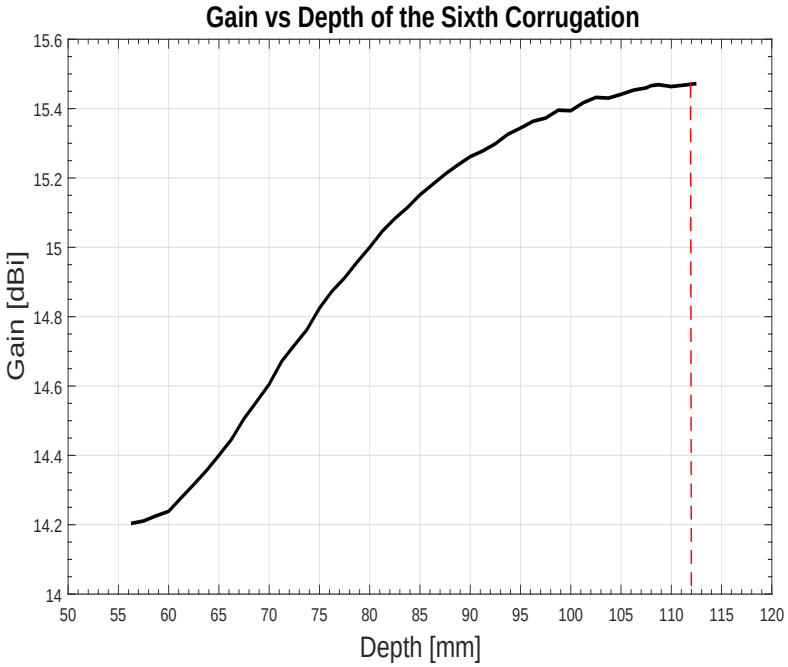

Figure 13: Gain vs Depth of the sixth corrugation

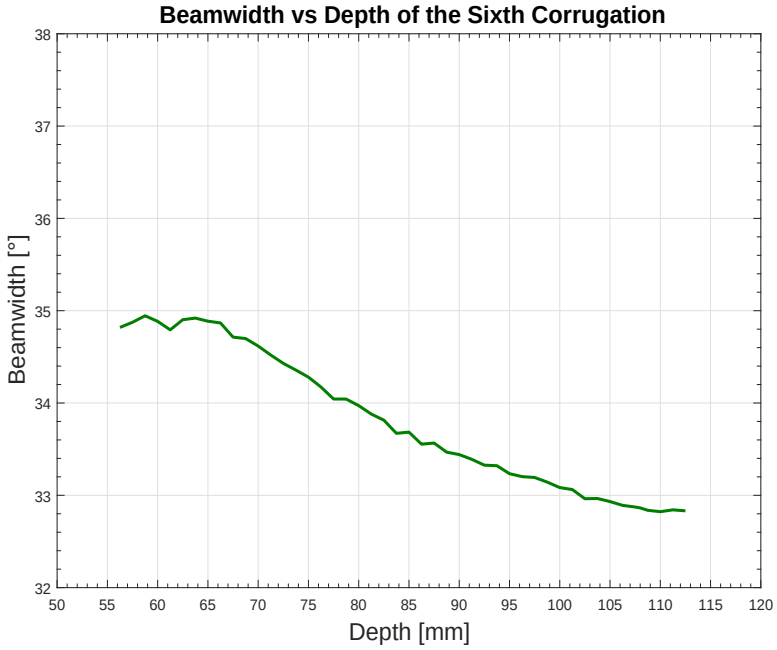

Figure 14: 3-dB Beamwidth vs Depth of the sixth corrugation

Figure 13 shows that the gain increments when the depth increases. The value choosen for the depth in this case is 112 mm, as it is pretty close to $\frac{\lambda_0}{2}$. The beamwidth in Figure 14 decreases while the depth increments. For 112 mm depth, the 3-dB beamwidth is 32.84°.

Seventh Corrugation Depth

Likewise, another parametric sweep has been performed to find the seventh corrugation depth that maximizes the gain of the antenna.

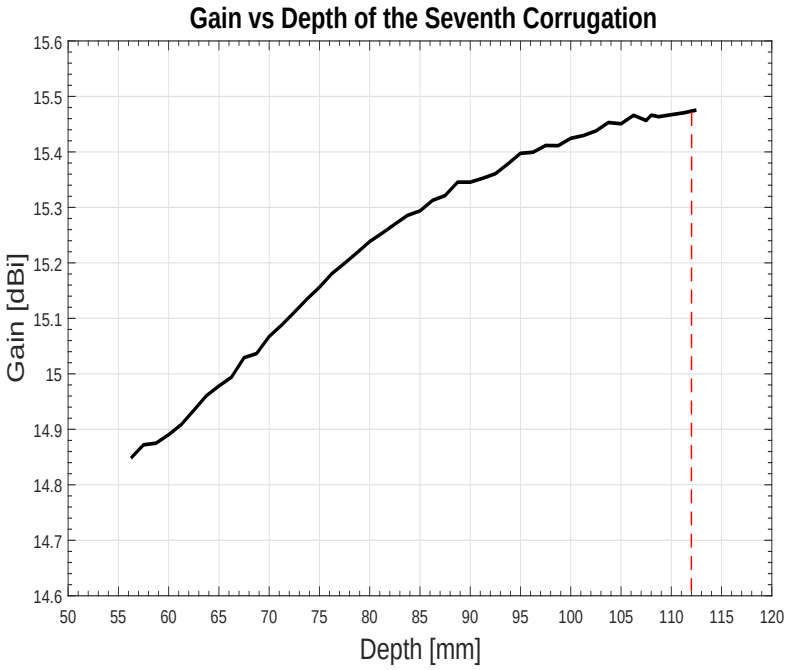

Figure 15: Gain vs Depth of the seventh corrugation

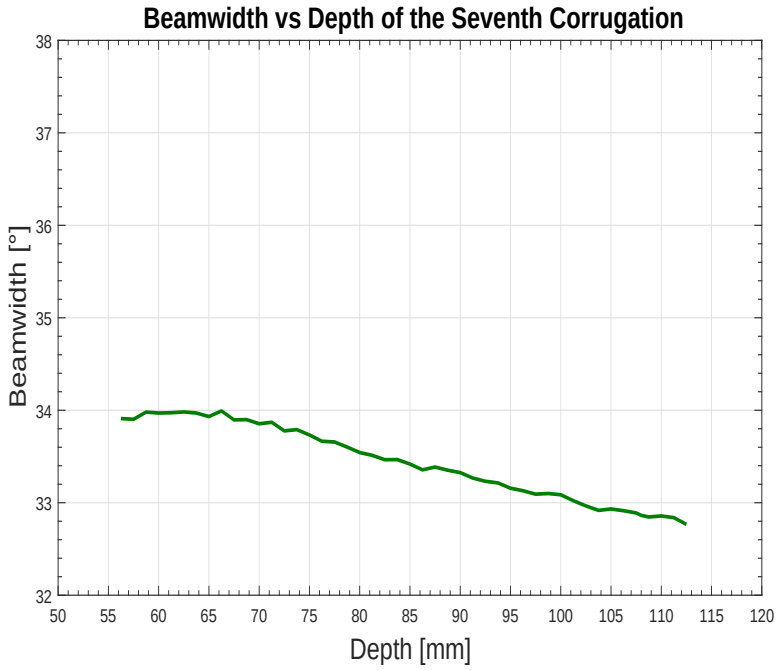

Figure 16: 3-dB Beamwidth vs Depth of the seventh corrugation

As in the previous two simulations, Figure 15 shows that the gain increments while the depth increases. The highest gain values can be obtained when the depth value is close to half-wavelength. Consequently the depth choosen is 112 mm. Respecting the 3-dB beamwidth, in Figure 16 it can been seen that the -3dB decreases while the depth increases and when the depth es equal to 112 mm, the -3dB beamwidth is 32.79°.

Eighth Corrugation Depth

For this simulation, a parameter sweep from $\frac{\lambda_0}{4}$ to $\frac{\lambda_0}{2}$ has been performed in order to find out which depth for the eighth corrugation gives the highest gain.

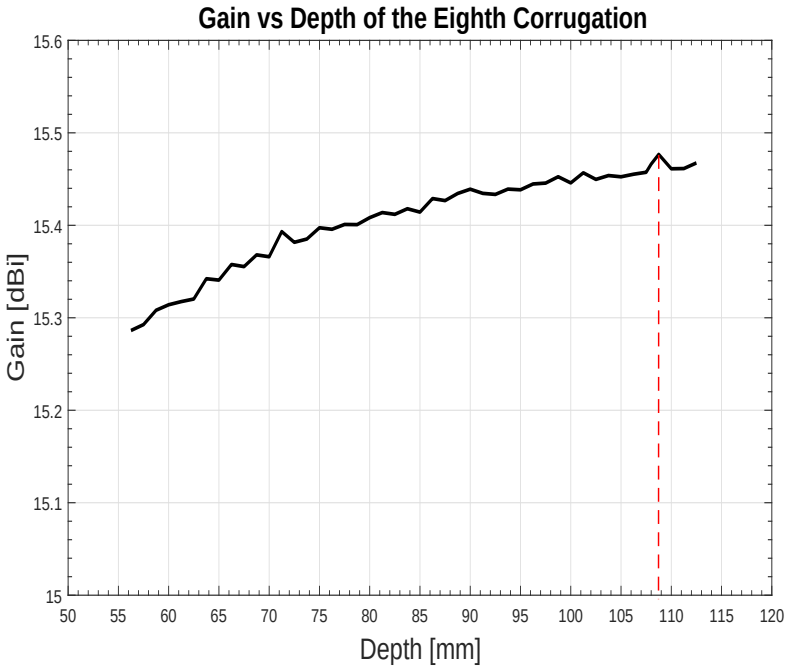

Figure 17: Gain vs Depth of the eighth corrugation

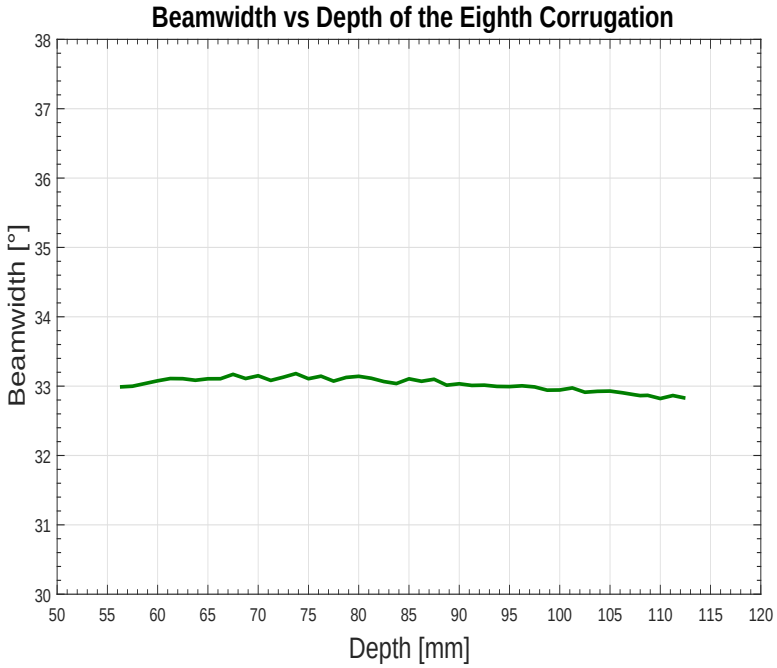

Figure 18: 3-dB Beamwidth vs Depth of the eighth corrugation

In Figure 17 is indicated that the highest gain obtained is 15.48 dBi for a 108.7 mm depth. As Figure 18 shows the beamwidth variation respect to the depth is not significant and the -3dB beamwidth which corresponds to this depth is 32.86°.

Ninth Corrugation Depth

Below, it is studied for which ninth corrugation depth, a higher gain can be obtained.

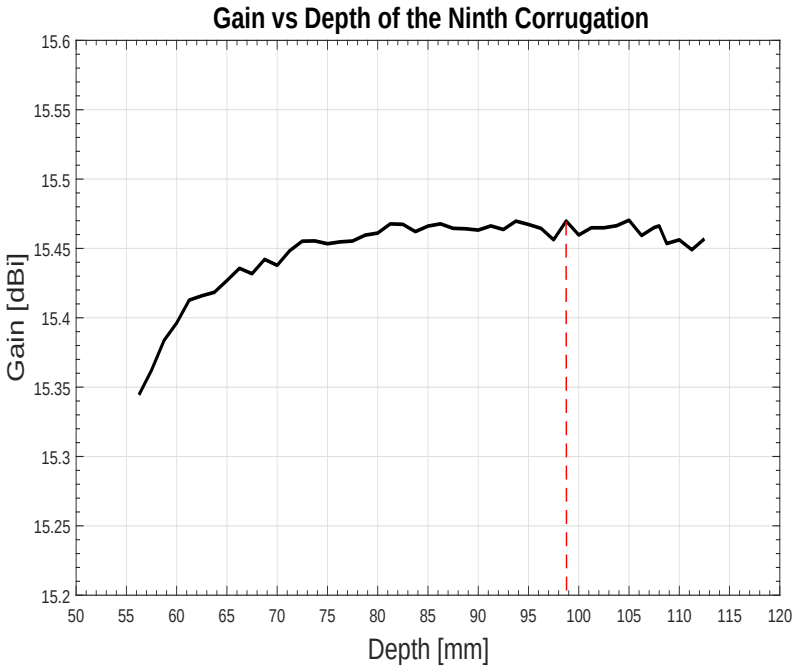

Figure 19: Gain vs Depth of the ninth corrugation

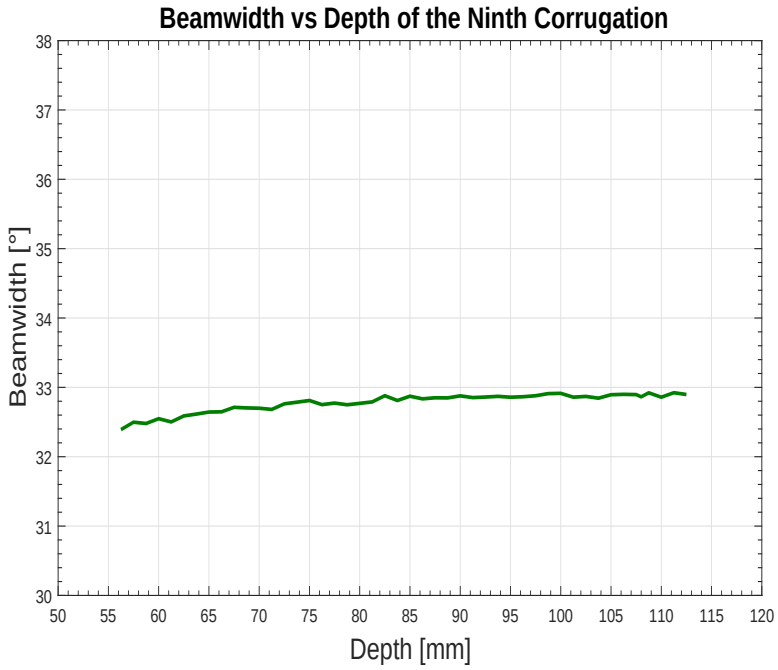

Figure 20: 3-dB Beamwidth vs Depth of the ninth corrugation

In Figure 19 is shown that the gain increments significantly until 80 mm depth, then it remains approximately constant. The maximum peak can be observed for 98.75 mm depth, when the gain is 15.47 dBi. Regarding the -3dB beamwidth, its variation respect to the depth is not significant, as it can be seen in Figure 20. For 98.75 mm depth, the -3dB beamwidth is 32.91°.

Tenth Corrugation Depth

For this simulation a parameter sweep has been performed in order to find out which tenth corrugation depth gives the highest gain.

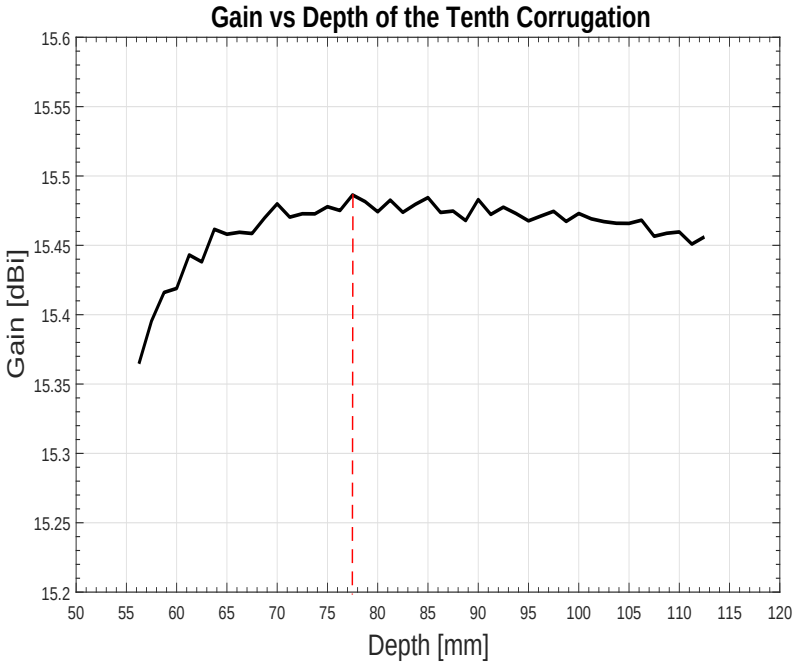

Figure 21: Gain vs Depth of the tenth corrugation

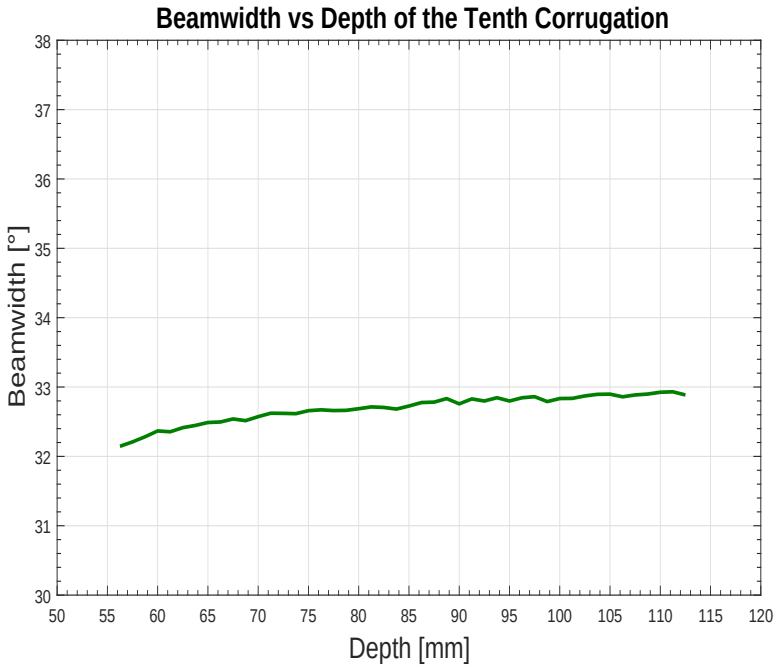

Figure 22: 3-dB Beamwidth vs Depth of the tenth corrugation

As it can be seen in Figure 21, the gain variation respect to the depth is not significant. The maximum value obtained is 15.49 dBi for 77.5 mm depth. Figure 22 shows that the -dB beamwidth remains approximately constant while the depth increments. If the tenth corrugation is 77.5 mm depth, the -3dB beamwidth will be 32.66°.

Eleventh Corrugation Depth

Another parameter sweep has been performed, this time for the depth of the eleventh corrugation from $\frac{\lambda_0}{4}$ to $\frac{\lambda_0}{2}$.

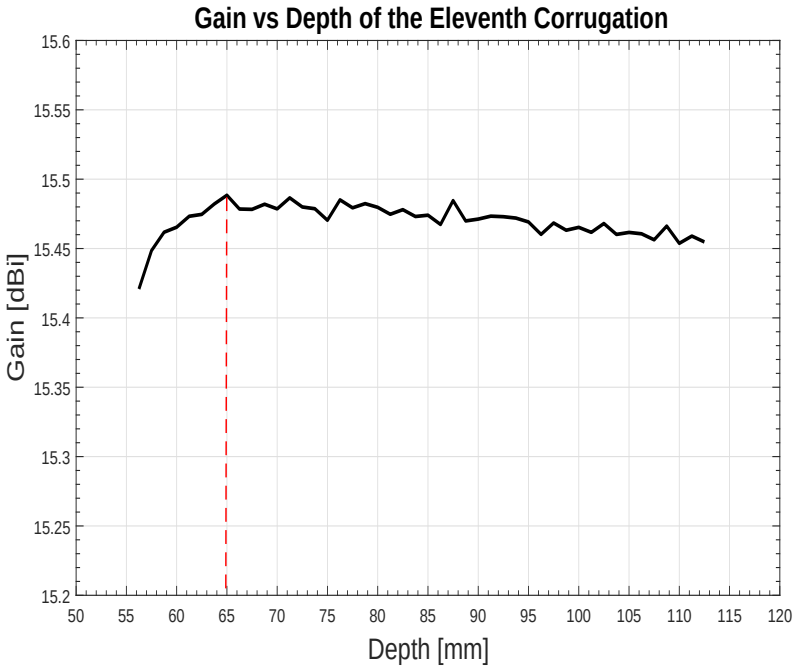

Figure 23: Gain vs Depth of the eleventh corrugation

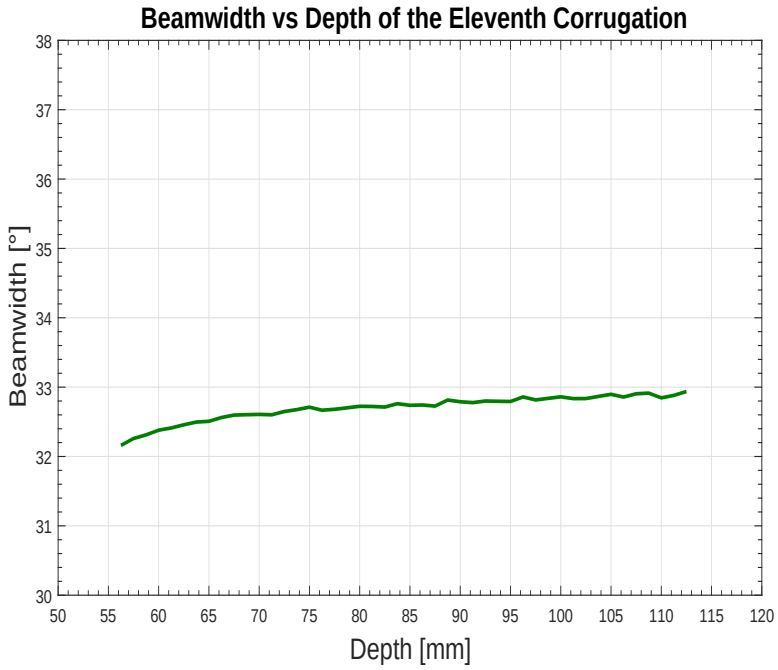

Figure 24: 3-dB Beamwidth vs Depth of the eleventh corrugation

In Figure 23 it can be seen that the gain takes values between 15.4 and 15.5 dBi while the depth increments from $\frac{\lambda_0}{4}$ to $\frac{\lambda_0}{2}$. The maximum value obtained is 15.49 dBi, for 64.94 mm depth. Figure 24 shows that the -3dB beamwidth variation respect to the depth is not significant. If the eleventh corrugation is 64.94 mm depth, the -3dB beamwidth will be 32.51°.

Twelfth Corrugation Depth

The last parameter sweep has been performed for depth of the twelfth corrugation, in order to find out which value of the depth maximizes the gain.

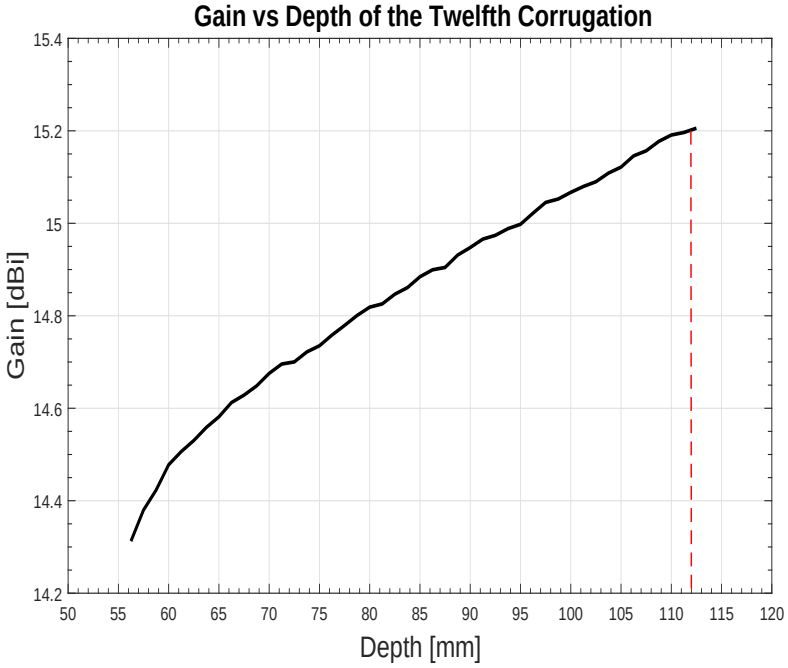

Figure 25: Gain vs Depth of the twelfth corrugation

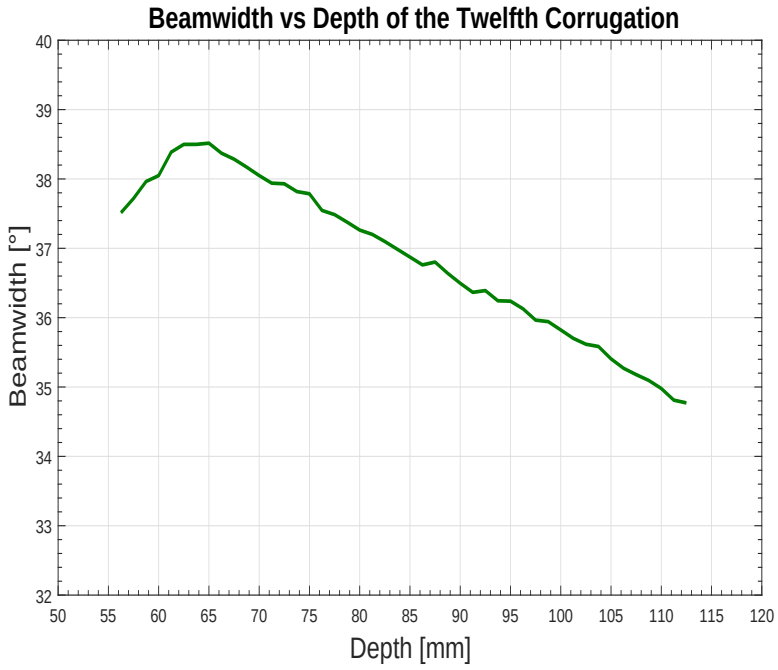

Figure 26: 3-dB Beamwidth vs Depth of the twelfth corrugation

In Figure 25 it can be observed that the gain increments linearly while the depth increases. Consequently, a depth value close to a half-wavelength must be chosen, for instance 112 mm. Regarding the -3dB beamwidth, Figure 26 shows that it decreases significantly while the depth increments. For the chosen depth, its value is 34.79°.

Conclusions and Results

Finally, in Table 4 the depths that maximize the gain of the antenna can be seen. In the simulations performed, it was observed that for the first corrugation, the better depth value is $0.25\lambda_0$. The depth of the second corrugation does not have a significant impact on the gain, but a value close to $0.5\lambda_0$ makes it higher. The third and the fourth corrugations depths should be close to $0.25\lambda_0$. For the next four corrugations, the depths should be as close as possible to $0.5\lambda_0$. The depths of the corrugations number nine, ten and eleven must not be close to $0.25\lambda_0$, but between $0.3\lambda_0$ and $0.5\lambda_0$ their influence on the gain is not significant. Finally, the depth of the last corrugation must be as close as possible to $0.5\lambda_0$.
In conclusion, the depths of the corrugations close to the aperture must be around $0.25\lambda_0$, while the depths of the corrugations near the junction must be approximately $0.5\lambda_0$.
Regarding the beamwidth, it was observed that for the first three corrugations, it remains approximately constant while the depths increase. From the fourth to the seventh corrugation and also for the last one, a decrease of maximum four degrees can be observed. Consequently, lower side lobes can be achieved if the depths of these corrugations are more close to $0.25\lambda_0$. From the eighth to the eleventh corrugations, the beamwidth does not have a significant variation respect to the depth.

Finally, in Table 6 the depths that maximize the gain of the antenna can be seen.

Table 4: Corrugations Depths

Corrugations	**Depth**
First corrugation	56.25 *mm*
Second corrugation	102.5 *mm*
Third corrugation	57.5 *mm*
Fourth corrugation	72.5 *mm*
Fifth corrugation	112 *mm*
Sixth corrugation	112 *mm*
Seventh corrugation	112 *mm*
Eighth corrugation	108.71 *mm*
Ninth corrugation	98.75 *mm*
Tenth corrugation	77.5 *mm*
Eleventh corrugation	64.94 *mm*
Twelfth corrugation	112 *mm*

Appendix 3: Tables containing the values of the depths of the corrugations

Table 5: Depths of the corrugations after the first genetic algorithm optimization

Parameter	**Symbol**	**Value**	**Units**
Depth of the second corrugation	D_2	66.39	mm
Depth of the third corrugation	D_3	80.88	mm
Depth of the fourth corrugation	D_4	71.66	mm
Depth of the fifth corrugation	D_5	96.54	mm
Depth of the sixth corrugation	D_6	105.82	mm
Depth of the seventh corrugation	D_7	92.80	mm
Depth of the eighth corrugation	D_8	80.53	mm
Depth of the ninth corrugation	D_9	77.73	mm
Depth of the tenth corrugation	D_{10}	85.19	mm
Depth of the eleventh corrugation	D_{11}	74.18	mm
Depth of the twelfth corrugation	D_{12}	110.15	mm

Table 6: Corrugations Depths after the second genetic algorithm optimization

Corrugations	**Depth**
First corrugation	56.25 *mm*
Second corrugation	100.58 *mm*
Third corrugation	56.25 *mm*
Fourth corrugation	89.55 *mm*
Fifth corrugation	106.23 *mm*
Sixth corrugation	103.20 *mm*
Seventh corrugation	106.20 *mm*
Eighth corrugation	107.39 *mm*
Ninth corrugation	105.78 *mm*
Tenth corrugation	93.38 *mm*
Eleventh corrugation	73.48 *mm*
Twelfth corrugation	105.56 *mm*

Table 7: Corrugations dimensions for a 10-corrugations horn

Parameter	**Symbol**	**Formula**	**Result**	**Units**
Width of the corrugations	w	$\frac{\lambda_0}{10}$	22.5	*mm*
Teeth of the corrugations	t	$\frac{w}{10}$	2.25	*mm*
Distance from the waveguide-horn junction	distance	$L_c - (10w + 10t)$	66.02	*mm*
Depth of the corrugations at the aperture	d_{aper}	$\frac{\lambda_0}{4}$	56.25	*mm*
Depth of the second corrugation	D_2	-	100.58	*mm*
Depth of the third corrugation	D_3	-	56.25	*mm*
Depth of the fourth corrugation	D_4	-	89.55	*mm*
Depth of the fifth corrugation	D_5	-	106.23	*mm*
Depth of the sixth corrugation	D_6	-	103.20	*mm*
Depth of the seventh corrugation	D_7	-	106.20	*mm*
Depth of the eighth corrugation	D_8	-	107.39	*mm*
Depth of the ninth corrugation	D_9	-	105.78	*mm*
Depth of the tenth corrugation	D_{10}	-	93.38	*mm*

Table 8: Depths of the 10 corrugations after optimization

Corrugations	**Depth**
First corrugation	56.25 *mm*
Second corrugation	78.86 *mm*
Third corrugation	63.65 *mm*
Fourth corrugation	68.36 *mm*
Fifth corrugation	102.44 *mm*
Sixth corrugation	98.68 *mm*
Seventh corrugation	110.80 *mm*
Eighth corrugation	96.36 *mm*
Ninth corrugation	77.56 *mm*
Tenth corrugation	76.23 *mm*

Table 9: Corrugations dimensions for a 14-corrugations horn

Parameter	**Symbol**	**Formula**	**Result**	**Units**
Width of the corrugations	w	$0.085\lambda_0$	19.12	*mm*
Teeth of the corrugations	t	$\frac{w}{10}$	1.91	*mm*
Distance from the waveguide-horn junction	distance	$L_c - (14w + 14t)$	18.99	*mm*
Depth of the corrugations at the aperture	d_{aper}	$\frac{\lambda_0}{4}$	56.25	*mm*
Depth of the second corrugation	D_2	-	100.58	*mm*
Depth of the third corrugation	D_3	-	56.25	*mm*
Depth of the fourth corrugation	D_4	-	89.55	*mm*
Depth of the fifth corrugation	D_5	-	106.23	*mm*
Depth of the sixth corrugation	D_6	-	103.23	*mm*
Depth of the seventh corrugation	D_7	-	106.20	*mm*
Depth of the eighth corrugation	D_8	-	107.39	*mm*
Depth of the ninth corrugation	D_9	-	105.78	*mm*
Depth of the tenth corrugation	D_{10}	-	93.38	*mm*
Depth of the eleventh corrugation	D_{11}	-	73.48	*mm*
Depth of the twelfth corrugation	D_{12}	-	105.56	*mm*
Depth of the thirteenth corrugation	D_{13}	-	87.01	*mm*
Depth of the fourteenth corrugation	D_{14}	-	57.13	*mm*